The Academy of Sciences of Belarus
A.V.Luikov Heat and Mass Transfer Institute

G.V.Miloshevsky

MONTE CARLO MODEL FOR NUMERICAL SIMULATION OF COMBINED PHOTON-ELECTRON TRANSPORT IN COMPOSITE TARGETS

Preprint No. 1

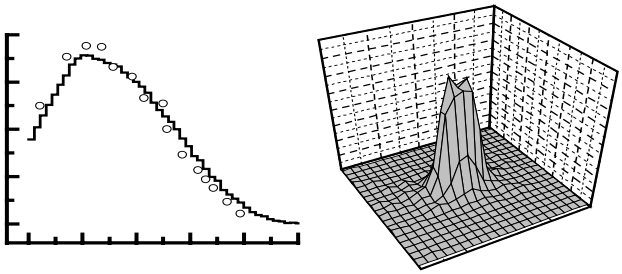

Minsk 1997

The theoretical model for numerical simulation of combined photon-electron transport in composite targets is presented. Description of physical processes taking place under action of high energy electrons or photons on the composite targets is given. Comparison of numerical results with experimental data is given also. Developed model was applied for numerical simulation of photon-electron transport in real atmosphere. Results of particle penetration through complex in geometry and chemical composition mediums are presented.

Introduction

At present the problem of penetration of fast particles through composite materials has great practical interest. It is bound up with problems arisen in new branches of science and technology. The range of such problems is rather wide: calculation of spatial energy distribution in composite targets, angular and energy spectrums of past and reflected particles, distribution of shift defects in solids and so on. Showers of secondary particles are generated in the result of incidence of high energy electrons or photons on the target. Secondary particles redistribute a part of energy of primary ones in a material. Thus, it is necessary to take into account the energy transfers by particles of all types in the result of collision processes.

This work presents the description of physical processes taking place under action of high energy electrons or photons on the composite targets. The considered energy range is from 5 keV up to 1 GeV. Type of interaction is determined by the forths which affect between the incident particle and scattering centers of medium. Electromagnetic interaction is described by the theory of quantum electrodynamics [1]. On the base of this theory the Monte Carlo model for numerical simulation of penetration of particles through complex in geometry and chemical composition mediums was developed. Physical model is formed in the approximation of binary collisions. It is supposed the incident particle interacts simultaneously with one scattering center (electron or nucleus) of medium. Scattering centers are placed by chance, i.e. the target is polycrystal. Interaction is occurred instantly in the collision point. Density of incident particles is such that their collective interaction is neglected. Each particle interacts with the target independently from another. Numerical simulation of the penetration of particles is performed by the Monte Carlo methods. In Sections 1 and 2 the fundamental physical processes accompanying

the penetration of particles through composite targets are discussed. In Sec. 3 the Monte Carlo simulation model is described, and in Sec. 4 the simulation results are presented.

1. Interaction processes of electrons and positrons with matter.

The following physical processes of electron or positron interaction with matter are taken into account: the bremsstrahlung emission, the elastic electron-nuclear and positron-nuclear scattering, the elastic electron-electron and positron-electron scattering, the energy losses for excitation and ionization. In addition the annihilation process is taken into account for positrons. The energy losses for bremsstrahlung emission predominate over that for ionization when the energy of an incident particle is greater $E_b \approx 600/Z$ MeV, where Z is the atomic number of stopping medium. The losses for emission originate mainly from the Coulomb interaction with the nuclei. For high energy particles it is the main form of energy losses in medium. The losses for ionization predominate by low energies. The interaction cross sections of charged particles with the medium atoms are rather large. Therefore, the particles undergo a great number of collisions on some length of its trajectory (about 10^5 per 1 mm).

The characteristic property of electron or positron interaction with the atoms is deflection of its propagation direction that originates mainly from elastic collisions with the nuclei. The energy transfer in this process is negligible small because of the large difference between the masses of the incident particle and nucleus. The elastic scattering on the nuclei is Z times more efficient than that on the electrons. The energy loss of charged particles in matter is due to the processes of ionization and excitation of the electron cloud surrounding the nucleus. The deflection of propagation direction in these processes is rather small. Hence, to describe the electron or positron transport in matter one can take into account independently the acts of energy transfer and scattering [2]. The deflection of propagation direction is Z times more efficient than the energy loss. Therefore, a charged particle many times changes its direction before stops.

1.1 The bremsstrahlung emission by relativistic electrons and positrons.

The photon emission by charged particles is due to the change of its direction by motion in the electric field of the nucleus. This process plays a significant role in the energy losses for high energy electrons or positrons. The differential cross section of bremsstrahlung may be obtained in the first-order Born approximation. In this case the initial and final kinetic energy E_k of an electron or positron must satisfy the condition: $E_k >> 0.5 \cdot m_e c^2 \cdot (Z/137)^2$, where m_e is the electron mass, c is the velocity of light in vacuum. In first-order approximation the bremsstrahlung cross section has the same form both the electrons and positrons. In more high-order approximations the symmetry is violated. The differential cross section for bremsstrahlung is described by the Bethe-Heitler relativistic formula [1]:

$$\frac{d\sigma_{br}}{d\omega\, d\Omega_\omega d\Omega_e} = \frac{Z(Z+1)\alpha r_e^2}{4\pi^2}\frac{p' m_e^4}{p\, q^4 \omega}\left\{\frac{q^2}{\eta\eta' m_e^2}\left(2\varepsilon^2 + 2\varepsilon'^2 - q^2\right) + q^2\left|\frac{1}{\eta} - \frac{1}{\eta'}\right|^2 - \right.$$

$$\left. - 4\left(\frac{\varepsilon}{\eta'} - \frac{\varepsilon'}{\eta}\right)^2 + \frac{2\omega q^2}{m_e^2}\left(\frac{1}{\eta'} - \frac{1}{\eta}\right) - \frac{2\omega^2}{m_e^2}\left(\frac{\eta'}{\eta} + \frac{\eta}{\eta'}\right)\right\}, \qquad (1.1)$$

where $d\Omega_\omega, d\Omega_e$ are the elements of solid angles for photon emission and charged particle scattering, ω is the photon energy, $\varepsilon, \varepsilon'$ are the full energies of a charged particle before and after interaction, p, p' are the momenta of a charged particle before and after interaction, α is the fine structure constant, r_e is the classical electron radius, $q = p' + k - p$ is the momentum transferred to the nucleus, k is the photon momentum, $\eta = \varepsilon - np$, $\eta' = \varepsilon' - np'$, $n = k/\omega$. The bremsstrahlung emission in the electric field of atomic electrons is taken also into account by this expression.

The integration of the cross section given in Eq.(1.1) over both the photon and charged particle directions is rather lengthy but may be obtained in the analytical form. The energy spectrum of the photons emitted in the bremsstrahlung process is continuous. The distance from the nucleus where the bremsstrahlung process is occurred has the important role. It is found that the bremsstrahlung emission is occurred

on the distance greater than the nucleus radius. Therefore, the nucleus may be considered as the point charge. However for low energy photons or for extremely high energy particles it is necessary to take into account the effect of screening by the atomic electrons. The effect of screening may be taken into account roughly by using of the potential $V(r) = (Ze/r)\exp(-r/a)$, where $a = 108Z^{-1/3}(\hbar/m_e c)$, e is the electronic charge, $\hbar$ is the Planck constant, r is the radial coordinate. This potential simulates screening by reducing the coulomb interaction for distant collisions. To take into account the effect of screening it is necessary in accordance with [3] to change the factor $\left(1/q^4\right)$ in Eq.(1.1) to $1/\left(q^2+\delta^2\right)^2$, where $\delta = Z^{1/3}m_e/108$.

The angular distribution of emitted photons is an energy function of the incident charged particles. If the particle energy is $\varepsilon \sim m_e$ then this distribution is uniform. In the case when the initial and final energies of the incident particle are high $(\varepsilon, \varepsilon' >> m_e)$ the emitted photon and emerging particle are occurred in the range $\theta \sim m_e/\varepsilon$.

The total cross section σ_{br} of the bremsstrahlung emission process is derived by the integration of Eq.(1.1) over $d\omega$, $d\Omega_\omega$ and $d\Omega_e$. The value σ_{br} determines the probability of the bremsstrahlung process. All characteristics (photon, electron or positron energies and directions) of particles taking part in the bremsstrahlung process are sampled on the base of the Monte Carlo model developed in [4].

1.2 The elastic electron-nuclear and positron-nuclear scattering.

It was mentioned above that this process gives main contribution into the deflection of charged particles. For the considered energy range the differential cross section of the elastic electron-nuclear or positron-nuclear scattering can be evaluated in the first Born approximation. In this approximation there is not difference in the electron and positron scattering. The differential cross section corresponding to the Coulomb potential Ze/r is described by the Mott formula [1]:

$$\frac{d\sigma_{en}}{d\Omega} = \frac{(Ze^2)^2\varepsilon^2}{4p^4}\frac{1-\beta^2\sin^2(\theta/2)}{\sin^4(\theta/2)}, \qquad (1.2)$$

where $\beta = v/c$, v is the particle velocity, θ is the scattering angle. This cross section is different from the Rutherford one when $\beta \sim 1$. From Eq.(1.2) one can see that there is large probability for scattering at small angles. The charged particles undergo a great number of far scatterings with small deflection on some trajectory length L. The scatterings at large angles (near scatterings) are rather seldom events. Therefore all scattering may be divided into two groups: near scatterings with deflection angle $\theta > \theta^*$ and far scatterings with $\theta < \theta^*$.

The near scatterings are described by the Eq.(1.2). The total cross section describing near scatterings is obtained by the integration of Eq.(1.2) over the angle θ in the range from θ^* up to π. Carrying out the integration over $d\Omega$, one obtains

$$\sigma_{en} = \pi \frac{\left(Ze^2\right)^2 \varepsilon^2}{p^4} \left[\frac{1+\cos\theta^*}{1-\cos\theta^*} + \beta^2 \ln\left| \frac{1-\cos\theta^*}{2} \right| \right]. \qquad (1.3)$$

When the near scattering is occurred the angle θ in the laboratory coordinate system is sampled from Eq.(1.2) by means of the Neumann method [5]. The energy transferred to the nucleus is determined from the relationship

$$\Delta T = 4 \frac{m_e M_n}{\left(m_e + M_n\right)^2} T \sin^2 \frac{\theta}{2},$$

where T is the kinetic energy of the incident particle, M_n is the nucleus mass. The value ΔT is negligible small.

The effect of far scatterings on the propagation direction accumulated on the length L can be considered in the following probabilistic approach. Due to the long-range Coulomb interaction the charged particle undergoes a great number of statistically independent collisions whose bulk effect is fully determined in terms of the mean deflection angle square

$$\left\langle \theta^2 \right\rangle = N_n L \int_{\theta<\theta^*} \theta^2 d\sigma_{en} \approx \frac{8\pi Z^2 e^4 \varepsilon^2}{p^4} N_n L \ln\left| \frac{\theta^*}{\theta_{min}} \right|, \qquad (1.4)$$

where N_n is the number density of medium atoms, $d\sigma_{en}$ is determined by Eq.(1.2), θ_{min} is the minimal deflection angle. θ_{min} is obtained using the Thomas-Fermi model: $\theta_{min} = Z^{1/3} \alpha \, m_e c / p$. The angle θ^* is cho-

sen from the condition that the summary deflection angle accumulated on the length L is small

$$\left\langle \theta^{*2} \right\rangle^{1/2} \approx \left(2\theta^{*} \ln\left| \frac{\theta^{*}}{\theta_{\min}} \right| \right)^{1/2} << 1.$$

The probability that the charged particle due to the far scatterings accumulates a deflection angle θ on the length L is determined from the Gauss distribution

$$P(\theta)d\theta = \frac{2\theta}{\left\langle \theta^{2} \right\rangle} \exp\left(-\theta^{2} \Big/ \left\langle \theta^{2} \right\rangle \right) d\theta. \qquad (1.5)$$

In the end of which length L the accumulated deflection angle θ is sampled from Eq.(1.5).

1.3 Kinetic energy loss of incident electrons in electron-electron collisions.

The atomic electrons of medium can be considered as free and to be at rest for the incident electrons with high kinetic energy. This assumption is fairly accurate because the character velocity of the atomic electrons is negligible compared to the high velocity of the incident electron. In the laboratory coordinate system the differential cross section of energy transfer to the atomic electron is written in the form [1]:

$$d\sigma_{\Delta} = 2\pi r_{e}^{2} \frac{d\Delta}{\gamma^{2}-1} \left[\frac{(\gamma-1)^{2}\gamma^{2}}{\Delta^{2}(\gamma-1-\Delta)^{2}} - \frac{2\gamma^{2}+2\gamma-1}{\Delta(\gamma-1-\Delta)} + 1 \right], \qquad (1.6)$$

where r_e is the classical electron radius, $\Delta = (T - T')/m_e$ is the kinetic energy transferred to the atomic electron in units of electron rest mass, T, T' are the kinetic energies of the incident electron before and after collision, $\gamma = T/m_e$. The identity of colliding electrons results in the occurrence of the so-called exchange interaction. This interaction has important role when the incident and recoil electrons have the energies of the same order in magnitude. The value Δ is changed in the range from 0 up to $(\gamma-1)/2$. In the result of the electron-electron collision the kinetic energy of the incident electron is decreased by the value $\Delta T = T - T'$ and the recoil electron with the kinetic energy ΔT is emerged. The vacancy is generated in an inner shell of the atom. Af-

terwards this vacancy is decayed either by means of the auger-electron ejection or photon emission. The cross section (1.6) is very large for low energy electrons, i.e. such electrons loss its energy in the place of their emergence. Therefore all electron collisions are divided into two groups: near collisions with energy transfer $\Delta > \Delta^*$ and far collisions with $\Delta < \Delta^*$, where $\Delta^* = \Delta T^* / m_e << 1$, ΔT^* is some value of kinetic energy of the recoil electron which is chosen to satisfy this condition.

Near collisions are treated as individual ones. It is convenient to consider the result of collision in the coordinate system of center inertia. The differential cross section of the near electron-electron collision is given by the relativistic Möller formula [1]

$$\frac{d\sigma_{ee}}{d\Omega} = r_e^2 \frac{m_e^2\left(\varepsilon_{ct}^2 + p_{ct}^2\right)^2}{4p_{ct}^4\varepsilon_{ct}^2}\left[\frac{4}{\sin^4\theta} - \frac{3}{\sin^2\theta} + \left|\frac{p_{ct}^2}{\varepsilon_{ct}^2 + p_{ct}^2}\right|^2\left(1 + \frac{4}{\sin^2\theta}\right)\right], \qquad (1.7)$$

where $p_{ct}^2 = m_e(\varepsilon - m_e)/2$, $\varepsilon_{ct}^2 = m_e(\varepsilon + m_e)/2$; $\varepsilon = T + m_e$ is the total electron energy in the laboratory coordinate system, θ is the scattering angle in the system of center inertia. The total cross section σ_{ee} of near electron-electron collisions may be obtained by the integration of Eq.(1.7) over the angle θ in the range from $\theta^* = \arccos\left(1 - 2\Delta T^*/T\right)$ up to π. The value σ_{ee} defines the probability of the near collision. If the near collision is occurred then the scattering angle θ is sampled from Eq.(1.7) by means of the Neumann method. After that in the laboratory coordinate system all characteristics are determined by the following expressions [6]

$$\Delta\varepsilon = \frac{\varepsilon - m_e}{2}(1 - \cos\theta); \quad \cos\vartheta_1 = \frac{(\varepsilon - \Delta\varepsilon)(\varepsilon + m_e) - \varepsilon m_e - m_e^2}{\left[\left(\varepsilon^2 - m_e^2\right)\left((\varepsilon - \Delta\varepsilon)^2 - m_e^2\right)\right]^{1/2}};$$

$$\cos\vartheta_2 = \frac{(\varepsilon + m_e)\Delta\varepsilon^{1/2}}{\left[\left(\varepsilon^2 - m_e^2\right)(\Delta\varepsilon + 2m_e)\right]^{1/2}}, \qquad (1.8)$$

where $\Delta\varepsilon$ is the total energy of the recoil electron, ϑ_1 is the scattering angle of the incident electron in the laboratory system, ϑ_2 is the angle between the incident and recoil electron directions in the laboratory system.

The energy loss of the incident electron in the result of far collisions when the kinetic energy of the recoil electron is less than ΔT^* is due to the processes of excitation and ionization. To calculate the energy loss of electrons in far collisions it is necessary to take into account that atomic electrons are bounded, i.e. to consider the system formed by the incident electron and atom. The theory for calculation of probability of different processes which cause the excitation and ionization was developed by Bethe. It is supposed the velocity of incident electron is much higher than the character bounded electron velocities, i.e. the first Born approximation is valid. Bounded electrons are detached by the Coulomb force impact produced by the incident electron. The differential electronic stopping power by detachment of bounded electrons can be written in the following form: $d\kappa_\Delta = Zm_e N_n \Delta d\sigma_\Delta$, where $d\sigma_\Delta$ is given by Eq.(1.6). The energy loss per unit length in far collisions is obtained by the integration of $d\kappa_\Delta$ over Δ in the range up to Δ^*. Performing the integration, one obtains

$$\left|\frac{dT}{dx}\right|_{ee} = \frac{2\pi Z\gamma^2}{\gamma^2-1} N_n m_e r_e^2 \left[\ln\left(\frac{\left(\gamma^2-1\right)m_e^2\Delta^*}{I^2}\right) - \left(\frac{2}{\gamma}-\frac{1}{\gamma^2}+1\right) \times \right.$$

$$\left. \times \ln\left| \frac{1}{1-\frac{\Delta^*}{2(\gamma-1)}} \right| + \frac{1}{1-\frac{\Delta^*}{2(\gamma-1)}} + \frac{1}{\gamma^2} + \frac{\Delta^{*2}}{8\gamma^2} - 2 \right|, \qquad (1.9)$$

where I is the average ionization potential. This parameter used in Bethe theory is formally defined by $Z \ln I = \sum_n f_n \ln E_n$, where E_n and f_n are the possible electronic energy transitions and corresponding dipole oscillator strengths for the medium atoms. In practice the oscillator strengths and the transition energies are not well enough known to simply calculate an I of sufficient accuracy. Therefore this value was found from quantum mechanically calculations in accordance with Hartree-Fock-Slater model [7,8]. Equation (1.9) takes into account both the small and large momentum transfers compared to momenta of the atomic electrons. The momentum transfer is always small compared to the initial momentum of the incident electron. In the result of far electron-electron collisions the kinetic energy of the inci-

dent electron traveled the length L is decreased by the value $\Delta T = L \cdot (dT/dx)_{ee}$.

1.4 Kinetic energy loss of incident positrons in positron-electron collisions.

In this case the identity of interacting particles is absent. Therefore there is some difference in electron-electron and positron-electron cross sections. The energy loss of positrons is considered also in the first-order Born approximation. In the laboratory coordinate system the differential cross section of energy transfer to the atomic electron is given by the following expression [1]

$$d\sigma_{pe} = 2\pi r_e^2 \frac{d\Delta}{\gamma^2 - 1} \left[\frac{\gamma^2}{\Delta^2} - \frac{2\gamma^2 + 4\gamma + 1}{\gamma + 1} \frac{1}{\Delta} + \right.$$

$$\left. + \frac{3\gamma^2 + 6\gamma + 4}{(\gamma + 1)^2} - \frac{2\gamma}{(\gamma + 1)^2} \Delta + \frac{1}{(\gamma + 1)^2} \Delta^2 \right], \qquad (1.10)$$

where $\Delta = (T_p - T_p')/m_e$ is the kinetic energy transferred to the atomic electron in units of electron rest mass, T_p, T_p' are the kinetic energies of the incident positron before and after collision, $\gamma = T_p/m_e$. The value Δ is changed in the range from 0 up to $\gamma - 1$. All positron-electron collisions are divided into two groups: far collisions with energy transfer $\Delta T < \Delta T^*$ and near collisions with $\Delta T > \Delta T^*$, where $\Delta T^* << m_e$ is some value of kinetic energy of the recoil electron.

Near collisions when the recoil electron gets some value of kinetic energy ΔT which exceeds ΔT^* are treated as individual ones. The positron-electron scattering is considered in the system of inertia center. The differential cross section is given by the Bhabha formula [1]

$$\frac{d\sigma_{pe}}{d\Omega} = \frac{r_e^2}{16} \frac{m_e^2}{\varepsilon_{ct}^2} \left[\frac{(\varepsilon_{ct}^2 + p_{ct}^2)^2}{p_{ct}^4} \frac{1}{\sin^4 \theta/2} - \frac{8\varepsilon_{ct}^4 - m_e^4}{p_{ct}^2 \varepsilon_{ct}^2} \frac{1}{\sin^2 \theta/2} + \right.$$

$$\left. + \frac{12\varepsilon_{ct}^4 + m_e^4}{\varepsilon_{ct}^4} - \frac{4p_{ct}^2 (\varepsilon_{ct}^2 + p_{ct}^2)}{\varepsilon_{ct}^4} \sin^2 \frac{\theta}{2} + \frac{4p_{ct}^4}{\varepsilon_{ct}^4} \sin^4 \frac{\theta}{2} \right], \qquad (1.11)$$

where $p_{ct}^2 = m_e(\varepsilon_p - m_e)/2$, $\varepsilon_{ct}^2 = m_e(\varepsilon_p + m_e)/2$; $\varepsilon_p = T_p + m_e$ is the total positron energy in the laboratory coordinate system, θ is the scattering

angle in the system of inertia center. The total cross section σ_{pe} is derived by the integration of Eq.(1.11) over the angle θ in the range from $\theta^* = \arccos\left(1 - 2\Delta T^*/T_p\right)$ up to π. The scattering angle θ is sampled from Eq.(1.11) by means of the Neumann method. After that in the laboratory coordinate system the energy transferred to the recoil electron, the scattered positron and recoil electron directions are determined by means of the expressions (1.8).

The energy loss in far positron-electron collisions is due to the processes of excitation and ionization. This part of energy loss is taken into account in the approximation of continues deceleration. The differential stopping power of positrons is written in the form: $d\kappa_{pe} = Zm_e N_n \Delta d\sigma_{pe}$, where $d\sigma_{pe}$ is given by Eq.(1.10). The energy loss per unit length in far collisions is derived by the integration of $d\kappa_{pe}$ in the range up to Δ^*. Carrying out the integration over Δ, one obtains

$$\left|\frac{dT}{dx}\right|_{pe} = \frac{2\pi Z\gamma^2}{\gamma^2-1} N_n m_e r_e^2 \left[\ln\left(\frac{2m_e\left(\gamma^2-1\right)\Delta T^*}{I^2}\right) - \frac{2\gamma^2+4\gamma+1}{\gamma^2(\gamma+1)}\frac{\Delta T^*}{m_e} + \right.$$

$$\left. + \frac{3\gamma^2+6\gamma+4}{2\gamma^2(\gamma+1)^2}\left|\frac{\Delta T^*}{m_e}\right|^2 - \frac{2\gamma}{3\gamma^2(\gamma+1)^2}\left(\frac{\Delta T^*}{m_e}\right)^3 + \frac{1}{4\gamma^2(\gamma+1)^2}\left(\frac{\Delta T^*}{m_e}\right)^4 - \frac{\gamma^2-1}{\gamma^2}\right|, \quad (1.12)$$

where I is the average ionization potential. The kinetic energy of the incident positron traveled the length L is decreased by the value $\Delta T = L \cdot \left(dT/dx\right)_{pe}$.

1.5 Positron-electron annihilation.

In the result of annihilation the positron-electron pair disappears and two photons are generated. The production of two photons is necessary to satisfy the momentum conservation law. It is convenient to consider the result of annihilation in the system of the inertia center. In this system the energy of positron, electron and two photons is the same. The differential cross section of annihilation is given by the following expression [1]

$$\frac{d\sigma_{an}}{d\Omega} = \frac{r_e^2 m_e^2}{4\varepsilon_{ct} p_{ct}} \left| \frac{\varepsilon_{ct}^2 + p_{ct}^2\left(1+\sin^2\theta\right)}{\varepsilon_{ct}^2 - p_{ct}^2\cos^2\theta} - \frac{2p_{ct}^4\sin^4\theta}{\left(\varepsilon_{ct}^2 - p_{ct}^2\cos^2\theta\right)^2}\right|, \quad (1.13)$$

where $p_{ct}^2 = m_e(\varepsilon_p - m_e)/2$; $\varepsilon_{ct}^2 = m_e(\varepsilon_p + m_e)/2$; $\varepsilon_p = T_p + m_e$ is the total positron energy in the laboratory system, θ is the angle between the positron and any photon directions. The total cross section of annihilation is derived by carrying out the integration of Eq.(1.13) over θ. Evaluation of the integration gives

$$\sigma_{an} = \pi r_e^2 \frac{1-v^2}{4v}\left| \frac{3-v^2}{v}\ln\frac{1+v}{1-v} - 2\left(2-v^2\right)\right|, \qquad (1.14)$$

where $v = \sqrt{\varepsilon_p^2 - m_e^2}\,/\varepsilon_p$. The value σ_{an} determines the annihilation probability. The angle θ is sampled from Eq.(1.13) by means of the Neumann method. If the annihilation process is occurred then all characteristics in the laboratory system are given by the following expressions [6]

$$\omega_1 = m_e + \varepsilon_p(1+\cos\theta)/2; \quad \cos\vartheta_1 = \frac{\omega_1(\varepsilon_p + 2m_e) - m_e\varepsilon_p - 2m_e^2}{\omega_1\sqrt{\varepsilon_p(\varepsilon_p + 2m_e)}};$$

$$\omega_2 = m_e + \varepsilon_p(1-\cos\theta)/2; \quad \cos\vartheta_2 = \frac{\omega_2(\varepsilon_p + 2m_e) - m_e\varepsilon_p - 2m_e^2}{\omega_2\sqrt{\varepsilon_p(\varepsilon_p + 2m_e)}},$$

where ω_1, ω_2 are the energy of photons, ϑ_1, ϑ_2 are the angles of photons with respect to the initial positron direction.

2. Interaction processes of photons with matter.

Photons traversing a matter is either absorbed or scattered by the atomic electrons. It is considered the photons with energy higher 1 keV. The main interaction processes of such photons with matter are the following: electron-positron pair production, Compton scattering and photoabsorption.

2.1 The production of an electron-positron pair by energetic photons.

The effect of pair production is in that a photon with energy higher $2m_e$ generates a positron-electron pair in the field of nucleus. In the result of pair production a photon disappears. This process predominates for high energy photons. The nucleus in the electric field of

which the pair production is occurred takes a part of the photon momentum. However the nucleus does not acquire a considerable energy because of its large mass. Therefore the sum of total electron and positron energies is equal to the initial photon energy. Due to the limitations of the first Born approximation the low energy limit of validity is $\left(Ze^2/\ v_+\right)<<1$ and $\left(Ze^2/\ v_-\right)<<1$, where v_+, v_- are the positron and electron velocity, respectively. The differential cross section for the production of an electron-positron pair of energy $\varepsilon_-, \varepsilon_+$ and momenta p_-, p_+ by a photon of momentum k is given by the expression [1]

$$\frac{d\sigma_{pair}}{d\Omega_- d\Omega_+ d\varepsilon_+} = \frac{Z^2 \alpha r_e^2}{4\pi^2} \frac{m^4}{q^4} \frac{p_- p_+}{\omega^3} \left\{ \frac{q^2}{\eta_- \eta_+ m^2} \left(2\varepsilon_-^2 + 2\varepsilon_+^2 - q^2\right) - q^2 \left| \frac{1}{\eta_-} + \frac{1}{\eta_+} \right|^2 + \right.$$

$$\left. + 4\left(\frac{\varepsilon_-}{\eta_+} - \frac{\varepsilon_+}{\eta_-} \right)^2 + \frac{2\omega q^2}{m^2} \left(\frac{1}{\eta_-} + \frac{1}{\eta_+} \right) - \frac{2\omega^2}{m^2} \left(\frac{\eta_-}{\eta_+} + \frac{\eta_+}{\eta_-} \right) \right| , \qquad (2.1)$$

where $d\Omega_-, d\Omega_+$ are the elements of solid angles for emitted electron and positron, $\omega = \varepsilon_- + \varepsilon_+$ is the initial photon energy, $q = p_- + p_+ - k$ is the momentum transferred to the nucleus, $\eta_\pm = \varepsilon_\pm - p_\pm \cos\theta_\pm$; θ_-, θ_+ are the electron and positron angles with respect to the initial photon direction.

The cross section of pair production is increased with Z as Z^2. Hence, this process is more effective for high-Z nuclei. Symmetry of Eq.(2.1) with respect to an electron and positron is the result of the first-order Born approximation. Shielding becomes important for photon energies of the order of $137Z^{-1/3}m_e c^2$ and can be taken into account approximately in accordance with [3] by replacing $\left(1/q^4\right)$ in Eq.(2.1) by $\left| 1/\left(q^2 + \delta^2\right)^2 \right|$, where $\delta = Z^{1/3} m_e / 108$.

The angular distributions of generated electron and positron depend essentially from the photon energy ω. In the case when $\varepsilon_\pm >> m_e$ the electron and positron are emerged at small angles of order of $\theta_\pm \sim m_e/\varepsilon_\pm$ with respect to the initial photon direction.

The probability of the pair production process is determined from the total cross section σ_{pair} which is obtained by carrying out the integration of Eq.(2.1) over $d\varepsilon_+, d\Omega_+$ and $d\Omega_-$. Energies and angles of emitted electron and positron are sampled from Eq.(2.1) on the base of the Monte Carlo model developed in [4].

2.2 Compton scattering.

When the photon energy is still higher then the average ionization potential of the medium atoms the Compton scattering is a predominant process. In the result of Compton scattering a photon interacting with an atomic electron changes its direction and transfers a part of its energy to an electron. This process predominates in the energy range 1 - 10 MeV for elements with low and mean atomic weights. The differential cross section of Compton scattering in the laboratory coordinate system is described by the Klein-Nishina-Tamm formula [1]

$$d\sigma_{com} = \pi r_e^2 \frac{m_e d\omega'}{\omega^2}\left[\frac{\omega}{\omega'} + \frac{\omega'}{\omega} + \left|\frac{m_e}{\omega'} - \frac{m_e}{\omega}\right|^2 - 2m_e\left(\frac{1}{\omega'} - \frac{1}{\omega}\right)\right|, \qquad (2.2)$$

where ω, ω' are the photon energies before and after scattering. The total cross section σ_{com} of Compton scattering is derived by the integration of Eq.(2.2) over $d\omega'$ in the range from $\omega/(1+2\omega/m_e)$ up to ω. The value σ_{com} characterizes the probability of Compton scattering. If the process of Compton scattering is occurred then the photon energy ω' is sampled from Eq.(2.2) by means of the Neumann method. The scattering angle ϑ in the laboratory system is determined from the following expression: $\cos\vartheta = \left(\omega\omega' - m_e(\omega - \omega')\right)/(\omega\omega')$.

2.3 Photoeffect.

The physical phenomena of photoeffect is in the following: the photon interacts with an orbital electron of atom in the result of which an electron ejected from an atomic level obtains energy. A released level of atom is closed hereinafter by one of outside electrons. The act of photoabsorption is finished by the emission of electromagnetic radiation or ejection of auger-electron. In the case of small photon energies the optical electrons take part in the photoabsorption process. But by increasing of photon energy the photoabsorption results to ejection

of electrons from more deep shells. When the photon energy coincides with the bond energy of electrons of the given shell the effective section of absorption has a resonant maximum. Therefore it is known [1] that the maximum section of photoprocesses is occurred near to thresholds of photoionization. The cross section of photoabsorption depends essentially from the charge of medium nuclei and photon energy. By increasing of the nucleus charge the absorption cross section is increased as Z^n, where n is changed in the range from 4 up to 5 depending on the photon energy. For low energies ($\omega < 0.2$ MeV) the absorption cross section is proportional to $1/\omega^3$. For high energies ($\omega > 0.5$ MeV) that is proportional to $1/\omega$. In a case of high energy photons the maximal absorption is occurred on the K-shell of atoms. Then the differential cross section of photoabsorption is written in the following form [1]

$$d\sigma_{ph} = \sigma_n(\omega)\sin^2\theta\cos\varphi(1+4\beta\cos\theta)d\Omega, \qquad (2.3)$$

where $d\Omega$ is the element of solid angle for an ejected photoelectron, θ,φ are the polar and azimuthal angles, σ_n is the cross section of photoabsorption on the corresponding shell, $\beta = v/c$, v is the photoelectron velocity. The values σ_n are determined in the result of quantum mechanically calculations in accordance with Hartree-Fock-Slater model [7,8]. The total photoabsorption cross section σ_{ph} is evaluated by carrying out the integration of Eq.(2.3) over $d\Omega$. This cross section determines the probability of photoabsorption process. The angles θ and φ are sampled from Eq.(2.3).

3. Monte Carlo Simulation Model.

A three-dimensional Monte Carlo simulation code MONSOL was developed to track the combined photon-electron transport in composite materials. The Monte Carlo calculation follows real physical processes. This method makes it possible to simulate the random trajectories of particles as real ones if the cross sections of interaction processes are known. The Monte Carlo approach is vital in determining different information for complex in geometry and chemical com-

position targets. It gives also the possibility to take into account the secondary particles. The random numbers are used in the Monte Carlo calculation for sampling of the trajectory elements (trajectory length, scattering angle) from corresponding probabilistic distributions. This method is discrete one. From this point of view it is applicable for a wide adoption on a computer. The Monte Carlo approach doesn't require formulation of the discrete model of corresponding transfer equation. The simulation model used in the present work is as follows.

3.1 Target.

The element of target is presented in the form of a cube or parallelepiped of arbitrary measurements. From such elements the target of arbitrary form may be constructed. The free space between different composite elements is allowable. The cube or parallelepiped covered all composite elements will present the target. The coordinate system is chosen in the following manner. It is supposed that the flux of particles is incident on the plane (Y, Z) of the target and propagated along the axis X. The individual spatial grid is introduced for each composite element of target. The lengths along the axes X, Y and Z are discretized and represented by the $I+1$, $J+1$ and $K+1$ mesh points x_i, y_j and z_k for each element of target, respectively. It is considered a spatial grid where the points x_i, y_j and z_k form the cell boundaries. Thus, each spatial cell is described by the numbers (i, j, k).

The mass density ρ_0 of medium atoms may be given in two ways: 1) as a constant within the boundaries of each element of target; 2) as a constant within the boundaries of each i-th layer of each target element. The composition of medium atoms may be given as constant within the boundaries of each element of target. The composition is given by means of the fractions by mass. The fraction by mass $w^{(i)}$ of the i-th component in the composition is the ratio of the mass of i-th component to the total mass of composition: $w^{(i)} = m^{(i)} / m_{tot}$. The number density of medium atoms for the i-th component is determined by the following expression: $N^{(i)} = w^{(i)} \rho_0 / \left(A^{(i)} M_0 \right)$, where $A^{(i)}$ is the atomic weight of the i-th component, M_0 is the mass of unit atomic weight .

3.2 Sampling of initial characteristics of the incident particles.

The initial energy of an incident particle may be given in three different ways: 1) as a monoenergetic value; 2) as an uniformly distributed value in the given energetic interval; 3) as an arbitrary spectral function of energy distribution. In first case all incident particles have the same value of energy. In second case the energy value is sampled from the interval $[\varepsilon_1, \varepsilon_2]$ in accordance with the following expression: $\varepsilon = \varepsilon_1 + \xi(\varepsilon_2 - \varepsilon_1)$, where ξ is an uniform random number in the range $0 \le \xi < 1$. In third case the energy value is sampled from spectral function by means of the Neumann method. Usually the high-energy particles sampling from such spectral functions (e.g. solar-flare spectrums) are occurred with the low probability. But high-energy particles can essentially influence on some calculated characteristics. To increase the quota of such particles the scheme with weight is used. The energy of particle is sampled uniformly from the interval $[\varepsilon_a, \varepsilon_b]$ as described above, where $\varepsilon_a, \varepsilon_b$ are the boundary values of energy within of which the spectral function $f(\varepsilon)[1/\mathrm{MeV}]$ is changed. When the energy ε is sampled the weight of particle is determined by the following expression: $W(\varepsilon) = (\varepsilon_b - \varepsilon_a) \cdot f(\varepsilon)$. Afterwards this value is used by calculation of required characteristics. The sum of the values $\varepsilon_n W_n$ over all N histories determines the mean energy of the incident flux: $\sum_{n=1}^{N} \varepsilon_n W_n = \langle \varepsilon \rangle$, where ε_n is the sampled energy on the n-th history, W_n is the weight of particle on the n-th history.

Polar and azimuthal angles of the incidence of particle on the target may be given also in three different ways: 1) as a monoangular value; 2) as an uniformly distributed value in the given angular interval; 3) as an arbitrary spectral function of angle distribution. The values of angles are sampled in the same way as in the previous case. The polar angle is measured from the plain surface (Y, Z) in the range from 0 up to 90^0 degrees. The azimuthal angle is measured clockwise from the axis Z in the range from 0 up to 360 degrees if to see along the axis X.

Particles can enter into the target either in the given point or uniformly on some square of the plain (Y,Z).

3.3 Simulation of photon trajectories.

The model of individual collisions [9] is used to describe the transport of photons. According to this technique all elementary interaction acts are treated as individual. The realization of this technique is in the construction of a great number of photon trajectories. These trajectories are some polygonal lines. Rectilinear parts of trajectories are photon paths between two sequential collisions. One from possible elementary interaction processes (pair production, Compton scattering or photoabsorption) takes place in each collision point. Then the photon is absorbed (pair production or photoabsorption) or moved (Compton scattering) in a new direction with new energy while the next collision is occurred.

Let us take that the photon is in the point r with coordinates (x,y,z) and penetrates in the direction Ω characterizing the direction cosines $(\alpha_x,\beta_y,\gamma_z)$. The Monte Carlo technique for simulation of the photon trajectory includes the following steps:

1. The initial energy and incidence angle of the photon are sampled from corresponding distributions.
2. The optical path s between two sequential collisions is sampled according to $s=-\ln\xi$.
3. For the cell (i,j,k) in which the point r is located the total macroscopic cross section $\sigma_{tot}^{(i,j,k)}$ is evaluated as the sum of pair production, Compton scattering and photoabsorption ones $\sigma_{tot}=\sigma_{pair}+\sigma_{com}+\sigma_{ph}$, where $\sigma_{pair}=N_n\sigma_{pair}$, $\sigma_{com}=ZN_n\sigma_{com}$, $\sigma_{ph}=ZN_n\sigma_{ph}$.
4. The length d to the nearest cell boundary in the direction Ω is determined. The optical thickness d^{opt} is evaluated as $d^{opt}=d\cdot\sigma_{tot}$.
5. If $s>d^{opt}$ and the photon is within the boundaries of any target element then a new value of s is evaluated as $s=s-d^{opt}$. In this case the photon enters into a new cell (i',j',k'). Further simulation is continued from step 3.

6. If $s \le d^{opt}$ then the coordinates of collision point is evaluated as $x' = x + L\alpha_x$, $y' = y + L\beta_y$, $z' = z + L\gamma_z$, where $L = s/\ _{tot}$.
7. The selection of the collision partner is made randomly according to the probability $^{(i)}/\ _{tot}$ for the photon to collide with the i-th atomic species, where $^{(i)}$ is the total macroscopic cross section for the i-th atomic species.
8. The process type is sampled according to the probability $_i/\ _{tot}$, where $_i$ are the macroscopic cross sections of possible processes. If the absorption process is occurred then the photon trajectory is stopped.
9. The energy transfer and scattering angle are sampled from the corresponding expressions of the sampled process. The new direction cosines are calculated using the following expressions:

$$\alpha'_x = \alpha_x \cos\theta + (\alpha_r - \alpha_x \cos\theta_r)\sqrt{(1-\cos^2\theta)/(1-\cos^2\theta_r)},$$

$$\beta'_y = \beta_y \cos\theta + (\beta_r - \beta_y \cos\theta_r)\sqrt{(1-\cos^2\theta)/(1-\cos^2\theta_r)},$$

$$\gamma'_z = \gamma_z \cos\theta + (\gamma_r - \gamma_z \cos\theta_r)\sqrt{(1-\cos^2\theta)/(1-\cos^2\theta_r)}, \qquad (3.1)$$

where θ is the scattering angle, $\alpha_r, \beta_r, \gamma_r$ are the direction cosines of a random vector which has the uniform probability of distribution, $\cos\theta_r$ is the angle cosine between the initial direction Ω and the random vector. If the scheme with weight was used then the transferred energy is multiplied by the weight W. After that the simulation procedure is continued from step 2.

The procedure described above is repeated until the photon loses all its initial energy or is absorbed. When the photon energy becomes smaller than some value ω_{min} this calculation sequence is stopped. All secondary photons are traced in a similar way. Monte Carlo simulation is performed by carrying out the above calculations on many test photons.

3.4 Simulation of electron and positron trajectories.

The classification model in collisions [10] is used to describe the transport of charged particles. It was mentioned above that charged particles have very large interaction cross sections with medium atoms

and undergo a great number of collisions on some trajectory length. Therefore the usage of the model of individual collisions requires an enormous amount of computer time. The main idea of the classification model is to divide all collisions into two groups: far and near. Due to the long-range Coulomb interaction a charged particle is deflected mainly at small angles with small energy transfers. The scattering at large angles is rather seldom events. Hence, there is the certain sense to divide all collisions into two groups: far and near. Parameters determining this division are some energy T^* in the energy loss processes and some angle θ^* in the processes of scattering. The great number of far statistically independent collisions is occurred on some trajectory length L limited by coordinates of two near collisions. Far collisions is described by the multiple scattering theory [11,12]. In the end of which length L the summary scattering angle and energy loss are sampled from the corresponding angular and energy distributions. Near collisions are treated as individual ones. The characteristics of particles after a near collision are determined from the differential cross sections of interaction.

Let us take that the charged particle is in the point r with coordinates (x,y,z) and penetrates in the direction Ω characterizing the direction cosines $(\alpha_x,\beta_y,\gamma_z)$. The Monte Carlo technique for simulation of the charged particle trajectory includes the following steps:

1. The initial energy and incidence angle of the charged particle are sampled from corresponding distributions.
2. The optical path s between two near collisions is sampled according to $s=-\ln\xi$.
3. In the case of electrons for the cell (i,j,k) in which the point r is located the total macroscopic cross section $\sigma_{tot}^{(i,j,k)}$ of near collisions is evaluated as the sum of bremsstrahlung emission, elastic electron-nucleus scattering and electron-electron energy transfer ones $\sigma_{tot}=\sigma_{br}+\sigma_{en}+\sigma_{ee}$, where $\sigma_{br}=N_n\sigma_{br}$, $\sigma_{en}=N_n\sigma_{en}$, $\sigma_{ee}=ZN_n\sigma_{ee}$. In the case of positrons the total macroscopic cross section $\sigma_{tot}^{(i,j,k)}$ of near collisions is evaluated as the sum of bremsstrahlung emission, elastic positron-nucleus scattering, positron-electron energy transfer

and annihilation ones $_{tot} = _{br} + _{en} + _{ep} + _{an}$, where $_{br} = N_n\sigma_{br}$, $_{en} = N_n\sigma_{en}$, $_{ep} = ZN_n\sigma_{ep}$, $_{an} = ZN_n\sigma_{an}$.

4. The length d to the nearest cell boundary in the direction Ω is determined. The optical thickness d^{opt} is evaluated as $d^{opt} = d_{tot}$.
5. If $s > d^{opt}$ and the charged particle is within the boundaries of any target element then a new value of s is evaluated as $s = s - d^{opt}$. In this case the charged particle enters into a new cell (i', j', k'). On the length d the energy loss because of the excitation and ionization processes is taken into account into the (i, j, k)-th cell in accordance with $\Delta\varepsilon = d \cdot (dT/dx)$, where (dT/dx) is given by Eq.(1.9) in the case of electrons or by Eq.(1.12) in the case of positrons. If the scheme with weight was used then the energy loss $\Delta\varepsilon$ is multiplied by the weight W. In the end of the length d the angle correction is performed by the value θ sampled from Eq.(1.5). The new direction cosines are calculated by means of Eqs.(3.1). Further simulation is continued from step 3.
6. If $s \le d^{opt}$ then the coordinates of collision point is evaluated as $x' = x + L\alpha_x$, $y' = y + L\beta_y$, $z' = z + L\gamma_z$, where $L = s/_{tot}$. On the length L the energy loss and angle correction are taken into account as described above. The new direction cosines are determined by using Eqs.(3.1). The energy loss is multiplied by the weight W in the case of the scheme with weight.
7. The selection of the collision partner is made randomly according to the probability $^{(i)}/_{tot}$ for the charged particle to collide with the i-th atomic species, where $^{(i)}$ is the total macroscopic cross section for the i-th atomic species.
8. The process type is sampled according to the probability $_i/_{tot}$, where $_i$ are the macroscopic cross sections of possible processes.
9. The energy transfer and scattering angle in a near collision are sampled from the corresponding expressions of the sampled process. The direction cosines are evaluated by using Eqs.(3.1). If the scheme with weight was used then the transferred energy is multiplied by the weight W. After that the simulation procedure is continued from step 2 .

The procedure described above is repeated until the charged particle loses all its initial kinetic energy. When the energy becomes smaller than some value T_{min} this calculation sequence is stopped. All secondary charged particles are traced in a similar way. Monte Carlo simulation is performed by carrying out the above calculations on many test charged particles.

There is some difficulty to choose correctly the length L between two near collisions. In the considering model this value is determined in the following manner. The total macroscopic cross section $_{tot}$ determines the mean length L between two near collisions. The length L must not be less some minimal value below which the multiple scattering theory is invalid. This value may not be very large such that the energy losses for ionization will be compared with the kinetic energy at the beginning of this length. It is necessary to choose the length L in such manner that the difference in the interaction cross section was negligible on this length. To take into account this situation the fictitious collisions are introduced. The fictitious collision is occurred with probability $_{f}/\ _{tot}$, where $_{f}$ is the fictitious macroscopic cross section. The value of $_{f}$ is determined from the condition that the energy losses would not be higher 10% of the kinetic energy at the beginning of the length L. If the fictitious collision takes place, then the particle energy and its direction are not changed. Introducing of fictitious collisions allows to take into account the large sampled values of lengths L.

3.5 Simulation characteristics.

The following characteristics may be obtained using the 3-D Monte Carlo code MONSOL:

I. *One-dimensional profiles and two-dimensional fields of deposited energy into the elements of target.* In the result of tracing of N histories there are some values of deposited energy $\Delta E_{i,j,k}$ [MeV] in each cell (i,j,k). In order to calculate the deposited energy $\Delta\varepsilon_{i,j,k}$ [MeV] per one incident particle it is necessary to divide the values $\Delta E_{i,j,k}$ [MeV] by the number of histories N. Dividing each value of $\Delta\varepsilon_{i,j,k}$ [MeV] by the corresponding cell volume $\Delta V_{i,j,k}$ [cm^3] one can obtain the distribu-

tion of deposited energy per one incident particle $(d\varepsilon/dV)_{i,j,k}$ $[MeV/cm^3]$ in the elements of target. The values $(d\varepsilon/dV)_{i,j,k}$ were averaged over N different collision histories. Usually the density of energy flux $P[MeV/(cm^2\,sec)]$ is given as an initial parameter. The initial flux of particles $F[part/(cm^2\,sec)]$ before the target (plain (Y,Z)) may be given either a constant or arbitrary spectral function. In the case of spectral function the average flux of particles is determined as $F = P\ f(T)/T\,dT$, where T is the kinetic energy of particle, $f(T)$ is the spectral function. The flux Φ $[part/sec]$ through the surface (Y,Z) is expressed as $\Phi = F \cdot L_y \cdot L_z$, where L_y, L_z are the target lengths along the axes Y and Z. The power density $(dQ/dV)_{i,j,k}$ $[W/cm^3]$ is evaluated by multiplying the values $(d\varepsilon/dV)_{i,j,k}$ and Φ. One-dimensional profile of deposited energy along the axis X is obtained by summation over indexes j and k. In the same way the corresponding profiles along another axes can be determined. Two-dimensional fields of deposited energy are obtained by summation over one of indexes.

II. *One- and two-dimensional distributions of produced ions.* It should be noted that the distributions of produced ions are easily determined if the energy deposition ones are known. It is supposed according to [13] that the total number of produced ions is proportional to the initial energy of an incident particle. Therefore the mean energy V_0 required to produce one pair of ions can be introduced. Then the ion production rate is given as the ratio of energy deposition to the mean energy V_0. One- and two-dimensional distributions of produced ions can be obtained by dividing the values $(dQ/dV)_{i,j,k}$ into the value V_0.

III. *One- and two-dimensional distributions of shift defects.* Fast particle penetrated into the matter undergoes collisions with the atoms. If the energy transferred to the atom is sufficiently high then the knocked-on atom is shifted from the node of crystal lattice. To shift the atom it is necessary to transfer the energy $\varepsilon_s \sim 25\,eV$. The shift defects are produced in the result of the elastic electron- and positron-nucleus scattering. The recoil nucleus can have a considerable energy

and produce new defects. The number of secondary knocked-on atoms per primary one is estimated as $N \approx \varepsilon_i/(2\varepsilon_s)$, where ε_i is the energy of the primary recoil atom. The number $N+1$ is added into the cell (i,j,k) where the formation of defects is occurred. One- and two-dimensional distributions of shift defects are obtained in the same way as in the case of energy deposition where the number of shift defects $\Delta N_{i,j,k}$ is used instead of the values $\Delta E_{i,j,k}$. In the case when the scheme with weight is used the number $N+1$ of shift defects is multiplied by the weight W.

IV. *Angular and energetic spectrums of past and reflected particles.* These characteristics can be easily obtained in the presented Monte Carlo procedure. When the particle crosses any boundary plain of any target element its energy and angle are fixed. The unity is added into the cells within which the fixed energy and angle are found. The averaging over all histories gives the angular and energetic spectrums of particles for each boundary plain of each element of target. If the scheme with weight is used the weight W instead of the unity is added into the corresponding cells.

4. Numerical results.

To check the physical model for calculation of the electron interaction with solid targets results of numerical simulation were compared with experimental data obtained in the ELDIS facility [14,15]. ELDIS is a powerful electron beam facility. Calculations were performed for three angle distributions shown in Fig.1. The angle is measured from the axis X which is perpendicular to the target surface. The kinetic electron energies E_t in the beam are 70, 130 and 250 keV for three cases, respectively. Comparison of the results for carbon target is presented in Fig.2. One can see the satisfactory agreement between calculated and experimental data.

This code was applied also to the cases in which electrons are injected into different materials. Electrons of energy of 1-MeV were assumed to be incident perpendicularly on planar solid targets. Comparison of Monte Carlo results with experimental [16] and calculated

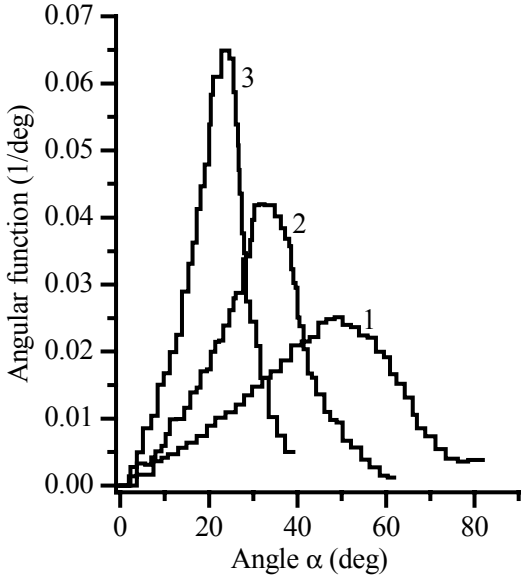

Fig. 1. Angle distributions of electrons with the axis X. 1-E_t=70 keV; 2-E_t=130 keV; 3-E_t=250 keV.

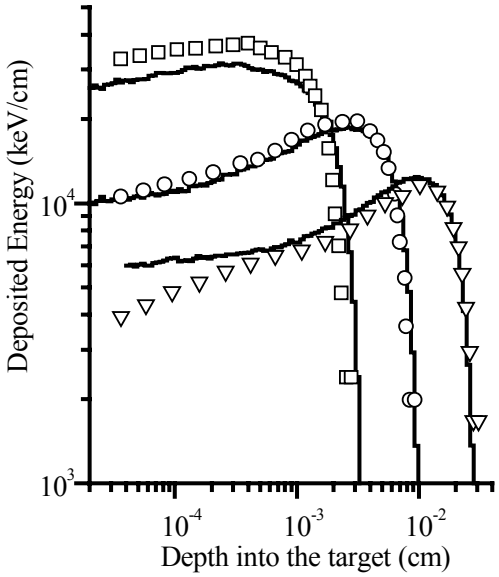

Fig. 2. Comparison of energy deposition for carbon target. Points - experimental data, curves - results of calculations. 1-E_t=70 keV; 2-E_t=130 keV; 3-E_t=250 keV.

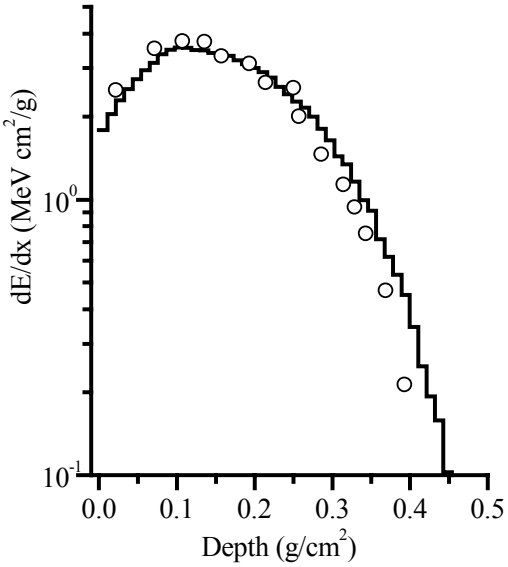

Fig. 3. Deposition profiles for 1-MeV electrons in aluminum. The curve represents the Monte Carlo result. The dots are experimental data [16].

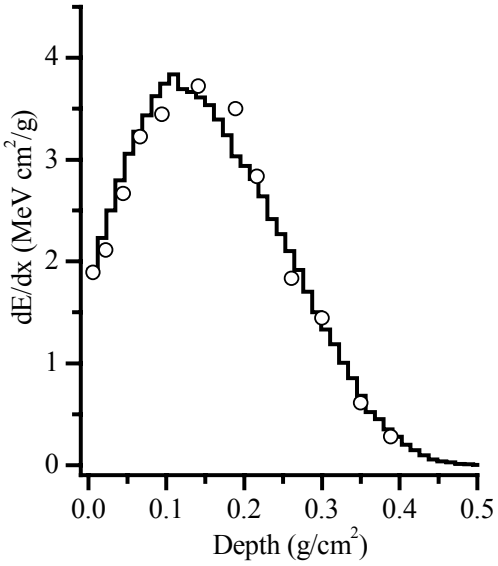

Fig. 4. Deposition profiles for 1-MeV electrons in silicon. The curve represents the Monte Carlo result. The dots are calculated data [17].

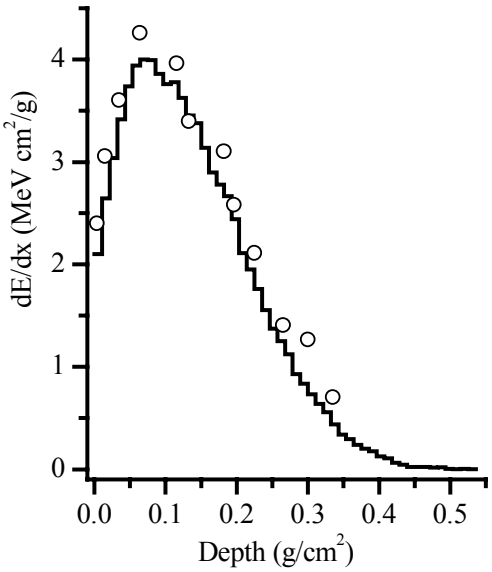

Fig. 5. Deposition profiles for 1-MeV electrons in copper. The curve represents the Monte Carlo result. The dots are calculated data [17].

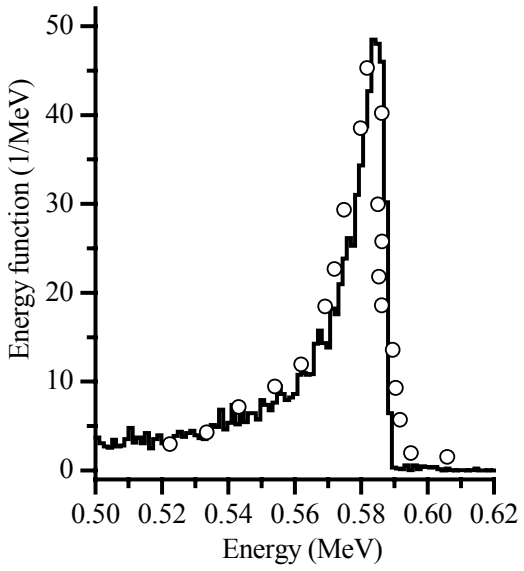

Fig. 6. Energy spectrum from 0.624-MeV electrons in gold target of thickness 38.35 mg/cm^2. The curve represents the Monte Carlo result. The dots are experimental data [18].

data [17] are presented in Figures 3, 4 and 5. The simulation results are in rather good agreement with the results of experiment and theory. Figure 6 shows the comparison of the energy spectrum from 0.624-MeV electrons in gold target of thickness 38.35 mg/cm^2 with experimental that derived from the β-spectrometer by Andreev [18].

The presented theoretical model was used for realization of the numerical experiment on passage of the photon-electron component through the atmosphere of the earth. The simulation was performed for a case when the electrons with energy equal to 1 GeV are incident on the top of the atmosphere. The space electrons with energy 1 GeV can enter into the atmosphere at the latitude 65^0 and greater. At smaller latitudes such electrons are strongly deflected by the magnetic field of the earth. The magnetic field of the earth does not allow the electrons with energy smaller some threshold to reach the atmosphere. Atmosphere inhomogeneity in the density and composition was taken into account. In the top-atmosphere the density of air is very low. Therefore in this atmosphere area the energy loss of incident electrons

originates mainly from ionization which is negligible small. Processes of electromagnetic collisions with the atmosphere atoms are occurred in the bottom-atmosphere below than 60 km. The origin and propagation of the photon-electron cascade are occurred in this atmosphere area.

The research of passage of the photon-electron shower is carried out in slab geometry in the area from height of 60 km and below. This height is assumed for a zero point. The flux of electrons with energy 1 GeV incident on the top-atmosphere is taken equal 30 electrons/(м^2·sec). The considered atmosphere area was divided into 1050 layers with a various step. The step is taken smaller near to the surface of the earth. In the boundaries of each layer the density of air is supposed constant. As the energy of an incident electron is rather high on the initial stage of origin of the cascade the secondary particles are ejected under very small angles with respect to direction of a primary electron. In the process of propagation of the shower there is its expansion in cross directions.

The distribution of ion production rate as a function of height is presented in Figure 7. The ion production rate was determined as described above. It is shown that the maximum ion production rate is occurred at height about 17 km above a sea level. Below this height a gradual attenuation of the photon-electron cascade is occurred. The minimal energy for electrons and positrons is taken equal 50 keV. On achievement of this energy a charged particle are considered absorbed. Electrons and positrons with energies smaller than the minimal energy are not considered. The minimal energy for photons is taken equal 1 keV. For electrons and positrons the minimal energy in 50 keV is sufficient to consider their absorbed by achievement of this energy. The path of these particles with such energy up to a complete stop is about 12 meters at the height in 40 km. In the bottom-atmosphere layers the path will be much less as the density of air is increased. The minimum size of a cell is taken equal 40 meters. Therefore there are all basis to consider electrons and positrons with energies smaller 50 keV absorbed in that cell in which they reach this energy. The average number of secondary particles arising in the considered energy ranges is about 852, of them 604 electrons, 233 photons and 15 positrons per

one primary electron. 33.5% initial kinetic energy of incident electrons is transformed to the electromagnetic radiation.

The energy spectra of electrons and photons produced by primary electrons allow to determine an average number of these particles in the given intervals of energies at certain heights. Such spectra are shown in Figures 8-10. The angular spectra of electrons and photons are presented in Figures 11-14.

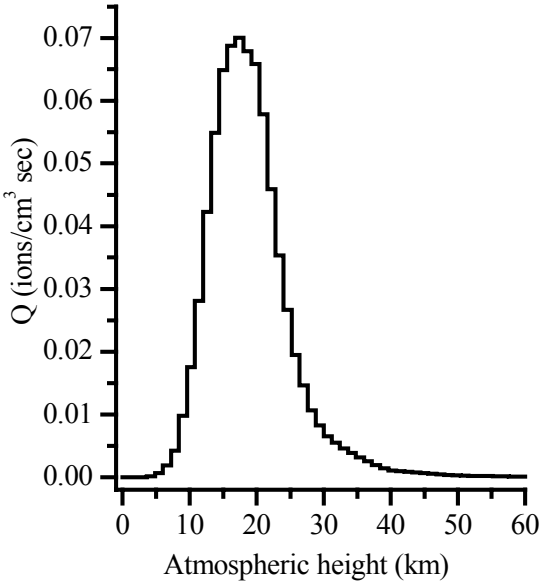

Fig. 7. Ion production rate Q as a function of height in the atmosphere for the photon-electron cascade.

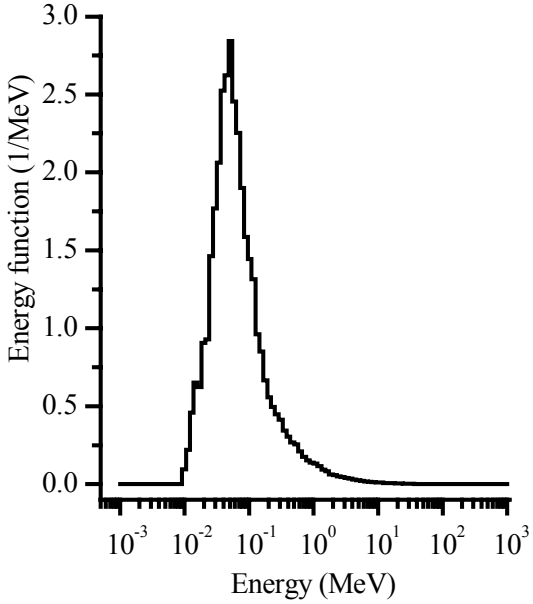

Fig. 8. Energy spectrum of photons in the atmosphere at height 24 km.

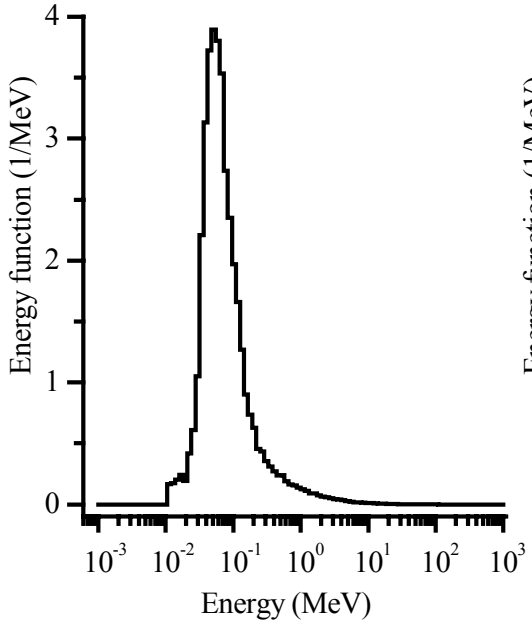

Fig. 9. Energy spectrum of photons in the atmosphere at height 14 km.

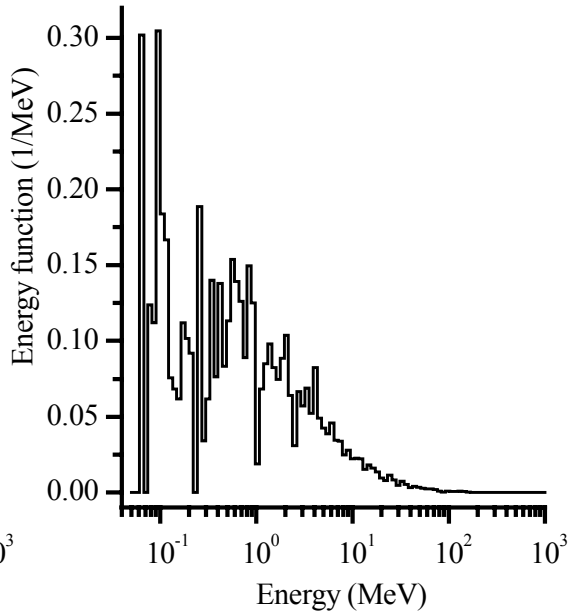

Fig. 10. Energy spectrum of electrons in the atmosphere at height 16 km.

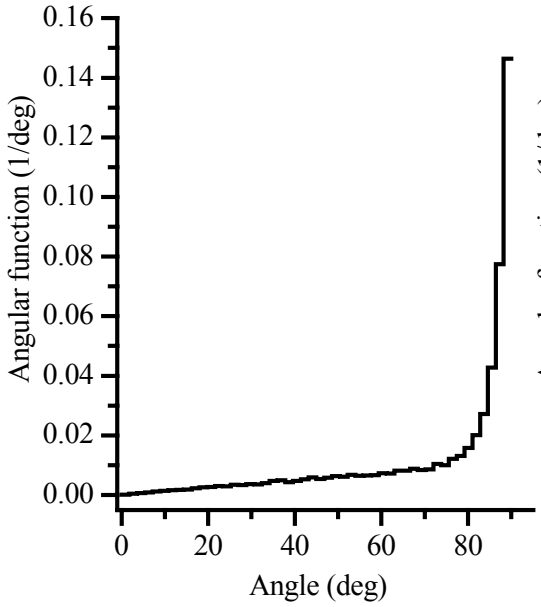

Fig. 11. Angular spectrum of photons in the atmosphere at height 22 km.

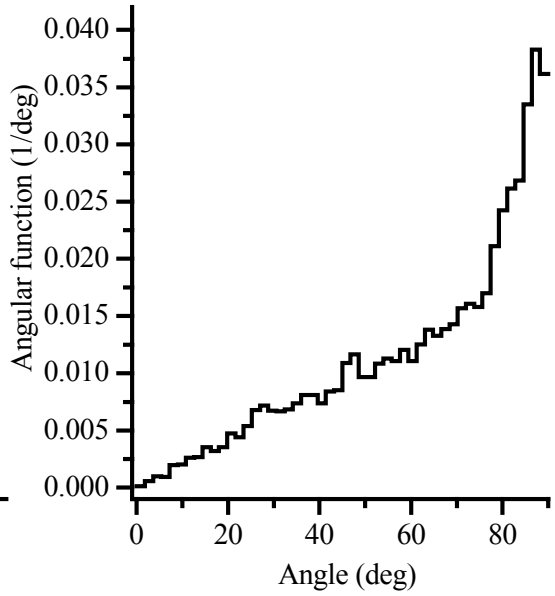

Fig. 12. Angular spectrum of photons in the atmosphere at height 12 km.

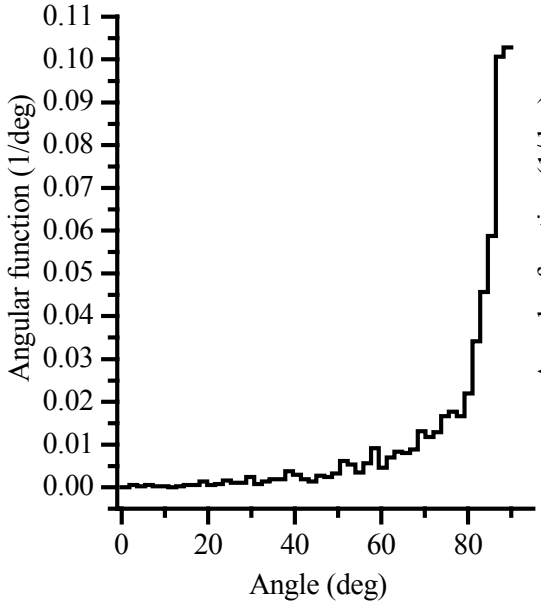

Fig. 13. Angular spectrum of electrons in the atmosphere at height 24 km.

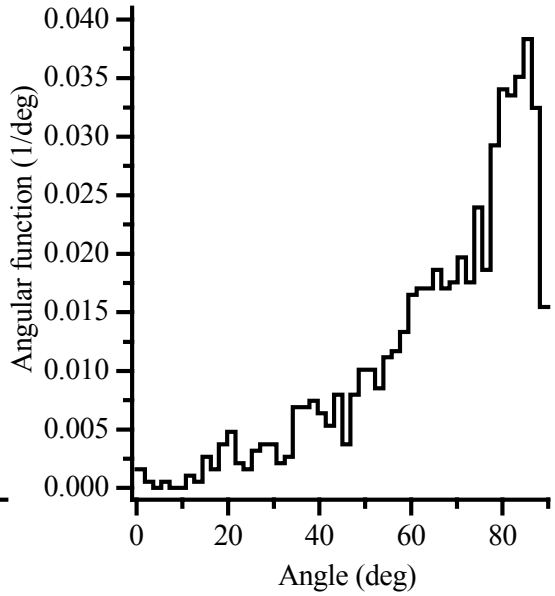

Fig. 14. Angular spectrum of electrons in the atmosphere at height 16 km.

The developed Monte Carlo model gives the possibility to investigate different aspects of radiating damages (failures) of semiconductor elements by particles of high energies. Many electronic devices consist of a plenty of semi-conductor cells with the sizes in a few hundreds μm and smaller. By action of high-energy radiation on the device the processes with participation of photons, electrons and positrons are occurred in its cells. In the result of passage of such cascade the medium of device is ionized and the failure of its work is taken place. The probability of frequency of failures of a semiconductor cell can be estimated if the value of energy deposited into it is known.

As a particular example the radiating damage by the electronic beam of an inhomogeneous microcircuit having the cross sizes 3x2 cm and consisting from 11 cells with different thickness was considered. A schematic view of a microcircuit is shown in Fig.15.

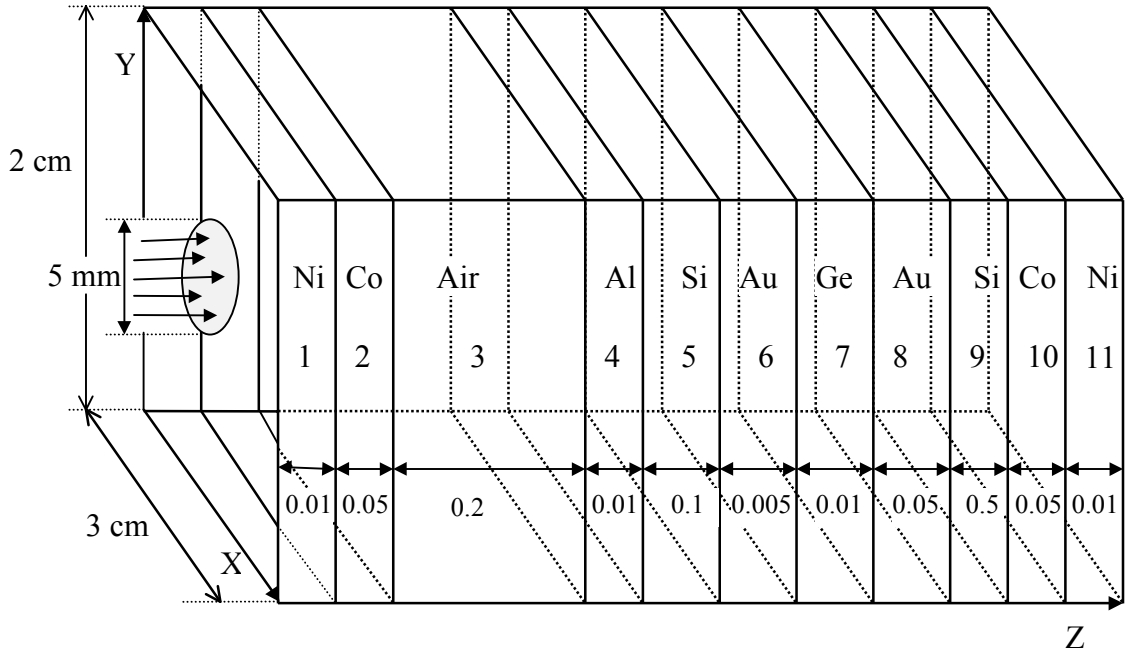

Fig. 15. Scheme of microcircuit. Numbers denote the thickness of cells in μm. The electron beam incident on the microcircuit surface is shown.

It was assumed that the electron beam with the radius 0.25 cm and the coordinates of center in the point (1.5;1 cm) is incident perpendicularly on the surface of a microcircuit. The electrons in the beam are distributed uniformly on the area of cross section. The energy spectrum of incident electrons is presented in Fig.16. The energy of an incoming electron is sampled from the given spectral function by means of the Neumann method. The scheme with weight described above was used to increase a portion of high-energy electrons. Energy flux of incident radiation was taken equal 10^3 MeV/(см^2 sec). It corresponds to the electron flux in 345,2 electr/sec through the (X,Y) surface of a microcircuit. In the result of tracing of 27800 histories the following results are obtained.

One-dimensional distribution of energy deposition into the cells of microcircuit is presented in Fig. 17. The average energy of electrons in the beam is equal 43.94 MeV. Total energy deposition in a microcircuit makes 8.3 MeV. 22.8% of average energy was transformed to electromagnetic radiation. Percentage of particles forming

the photon-electron cascade is the following: 34,8% of photons, 65,1% of electrons and 0,1% of positrons. The low boundary on energy for all particles was taken equal 1 keV. In volume of each cell making a microcircuit the following values of energy was deposited: 1 - 0.54 MeV, 2 - 1.89 MeV, 3 - 0.001 MeV, 4 - 0.1 MeV, 5 - 0.9 MeV, 6 - 0.28 MeV, 7 - 0.16 MeV, 8 - 0.24 MeV, 9 - 3.14 MeV, 10 - 0.9 MeV, 11 - 0.16 MeV. Comparing these values with threshold energy [19] describing radiative stability it is possible to predict the damage of considered cells.

Two-dimensional surfaces of energy deposition are shown in Figs.18-25 for different cells of a microcircuit. The energy and angular spectra of electrons and photons are shown in Figs.26-41.

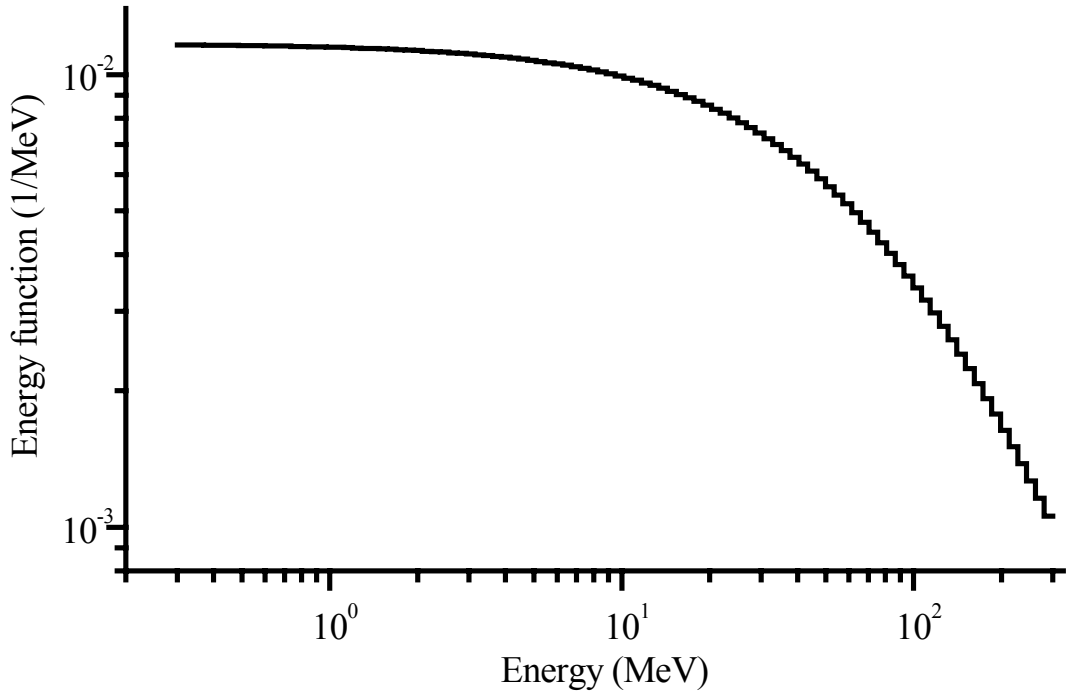

Fig. 16. Energy spectrum of incident electrons.

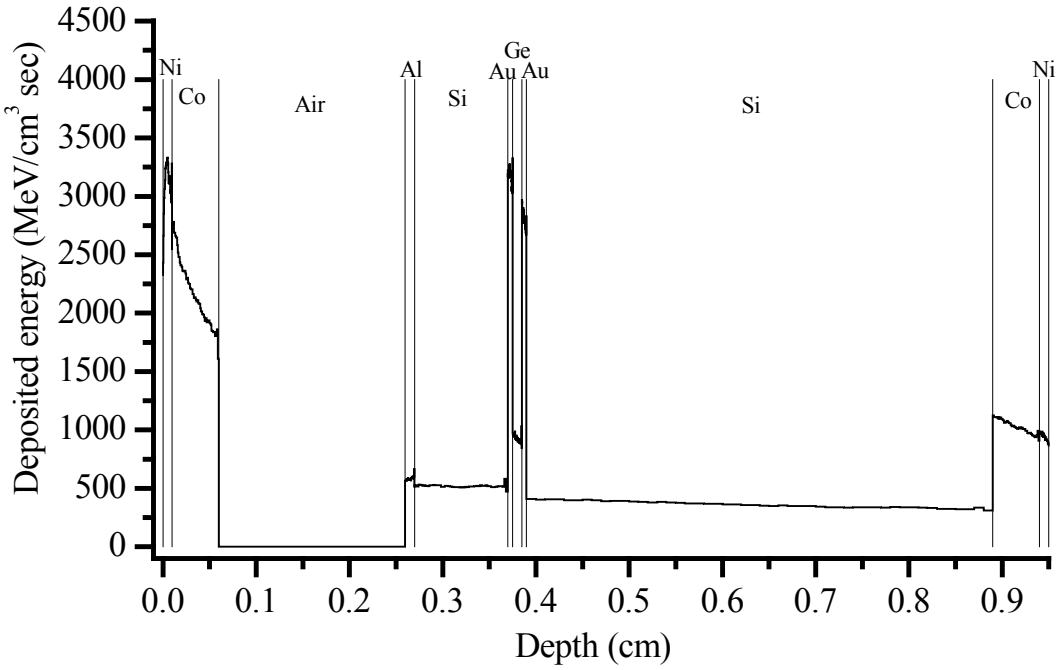

Fig. 17. Distribution of energy deposition in the microcircuit.

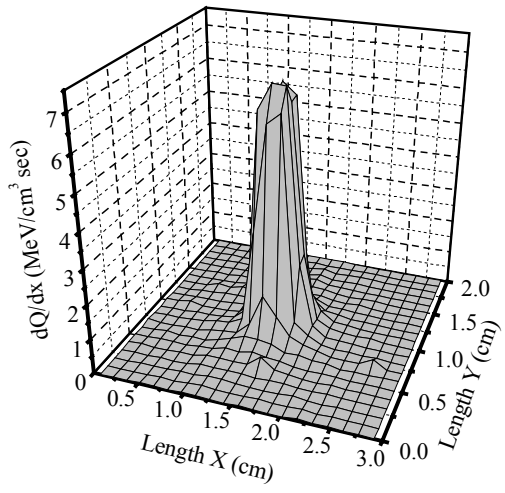

Fig. 18. Two-dimensional surface of energy deposition into 3-rd cell (Air) of a microcircuit.

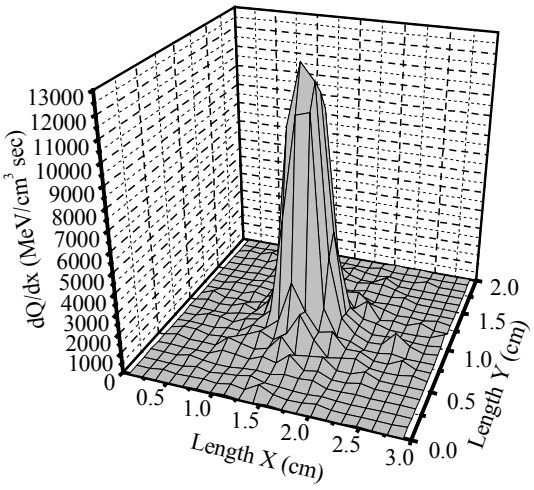

Fig. 19. Two-dimensional surface of energy deposition into 4-th cell (Al) of a microcircuit.

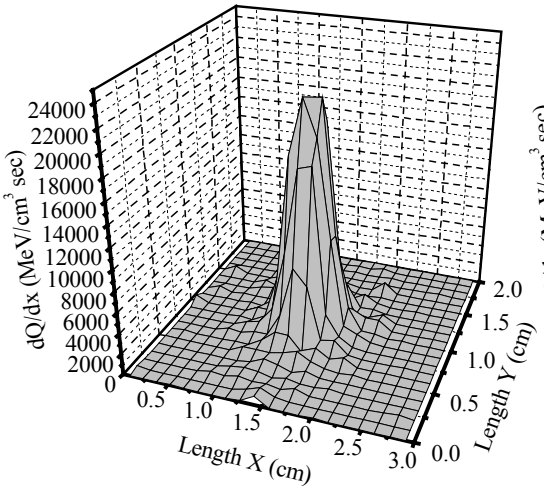

Fig. 20. Two-dimensional surface of energy deposition into 7-th cell (Ge) of a microcircuit.

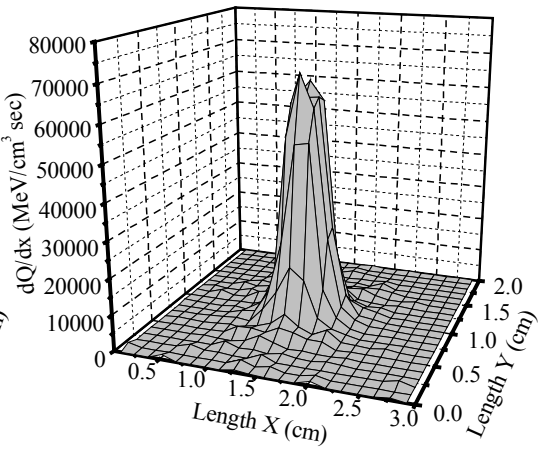

Fig. 21. Two-dimensional surface of energy deposition into 8-th cell (Au) of a microcircuit.

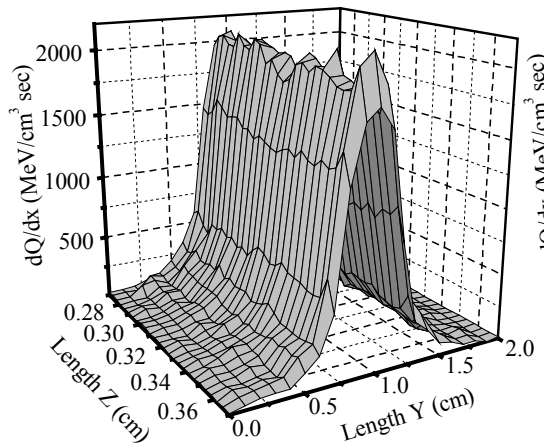

Fig. 22. Two-dimensional surface of energy deposition into 5-th (Si) cell of a microcircuit.

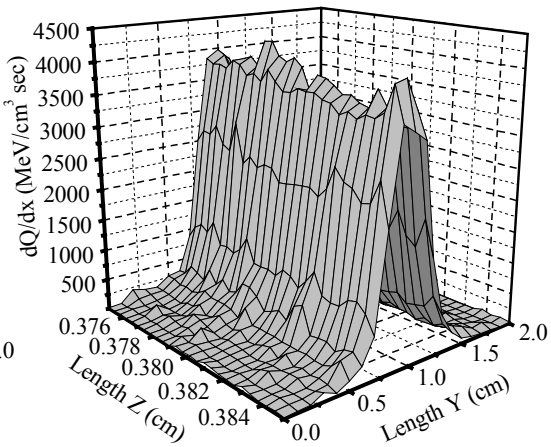

Fig. 23. Two-dimensional surface of energy deposition into 7-th (Ge) cell of a microcircuit.

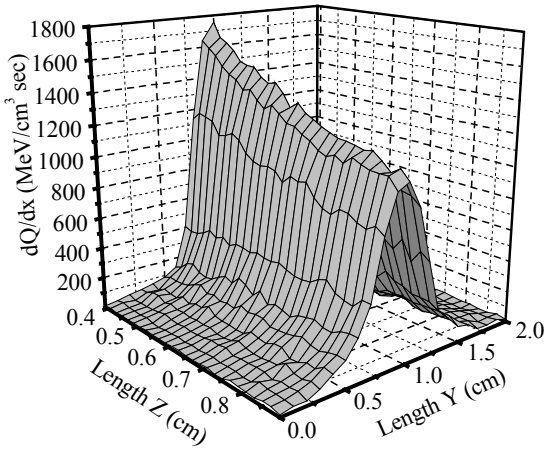

Fig. 24. Two-dimensional surface of energy deposition into 9-th cell (Si) of a microcircuit.

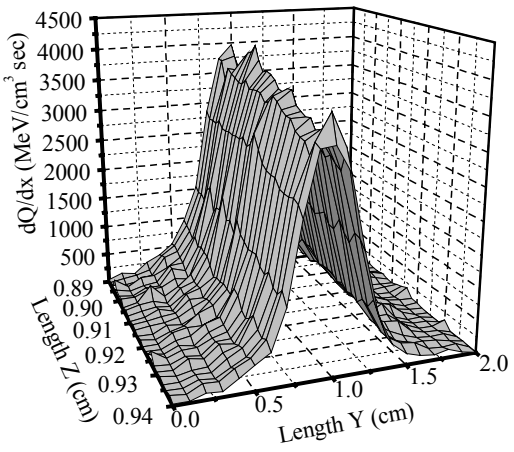

Fig. 25. Two-dimensional surface of energy deposition into 10-th cell (Co) of a microcircuit.

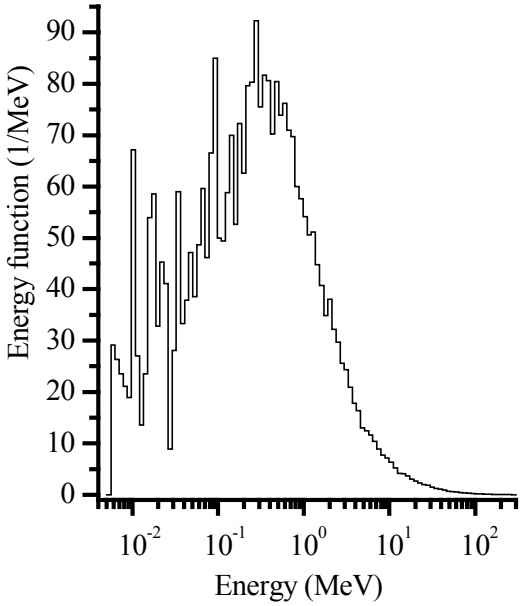

Fig. 26. Energy spectrum of electrons at the depth of 0.01 cm (after 1-st cell) in a microcircuit.

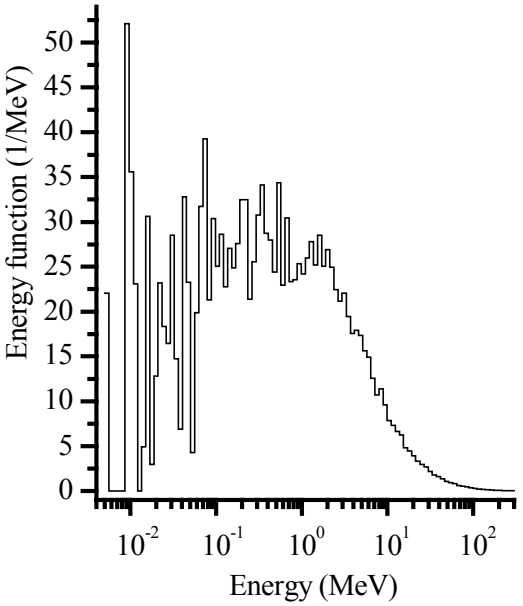

Fig. 27. Energy spectrum of electrons at the depth of 0.37 cm (after 5-th cell) in a microcircuit.

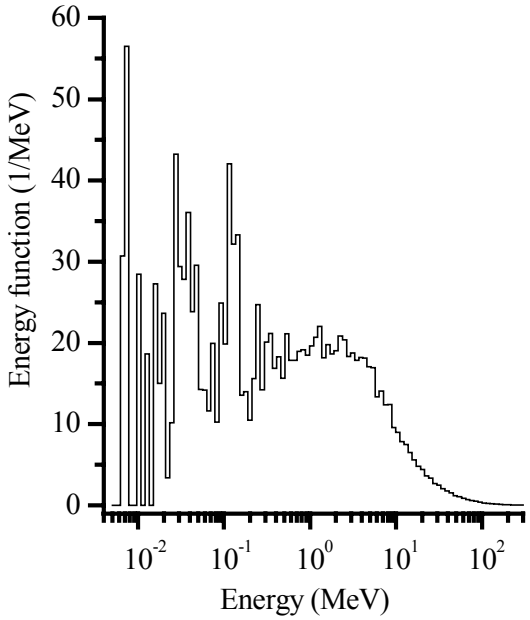

Fig. 28. Energy spectrum of electrons at the depth of 0.39 cm (after 8-th cell) in a microcircuit.

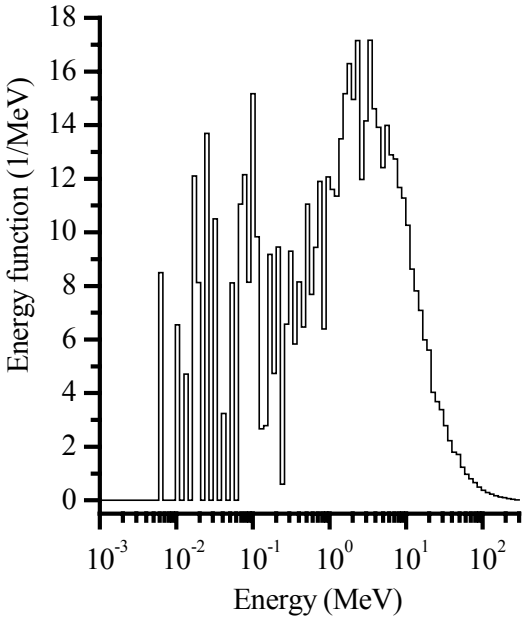

Fig. 29. Energy spectrum of electrons at the depth of 0.95 cm (after 11-th cell) in a microcircuit.

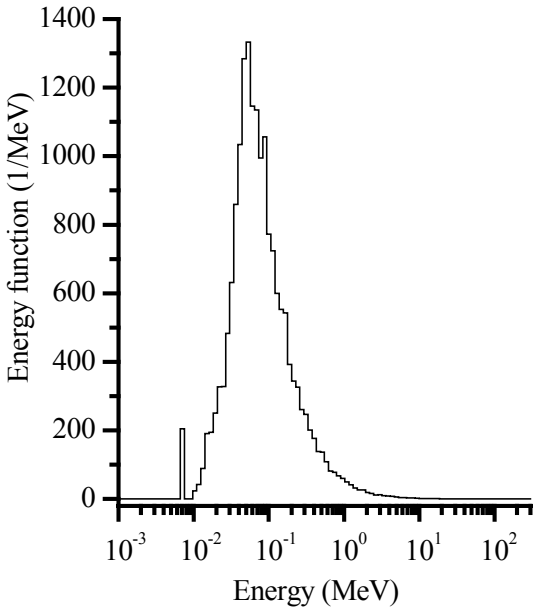

Fig. 30. Energy spectrum of photons at the depth of 0.26 cm (after 3-rd cell) in a microcircuit.

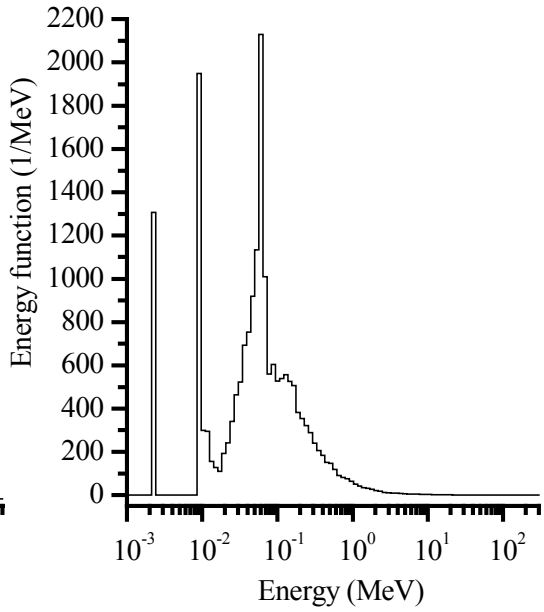

Fig. 31. Energy spectrum of photons at the depth of 0.375 cm (after 6-th cell) in a microcircuit.

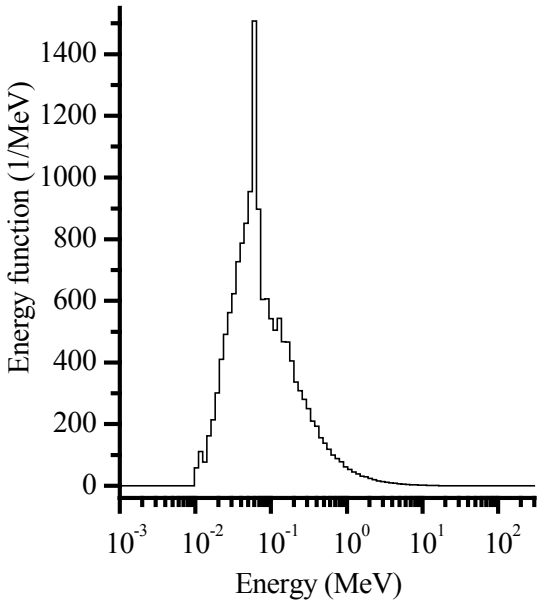

Fig. 32. Energy spectrum of photons at the depth of 0.89 cm (after 9-th cell) in a microcircuit.

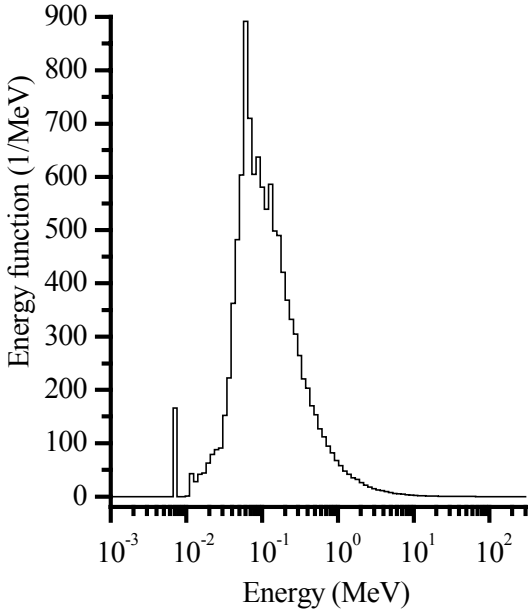

Fig. 33. Energy spectrum of photons at the depth of 0.95 cm (after 11-th cell) in a microcircuit.

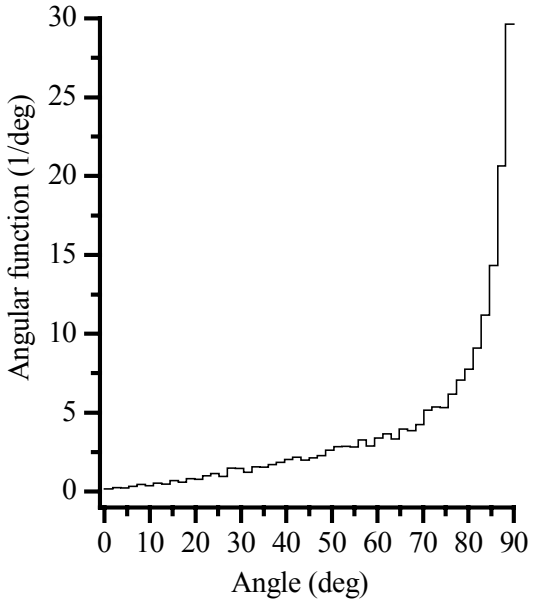

Fig. 34. Angular spectrum of electrons at the depth of 0.01 cm (after 1-st cell) in a microcircuit.

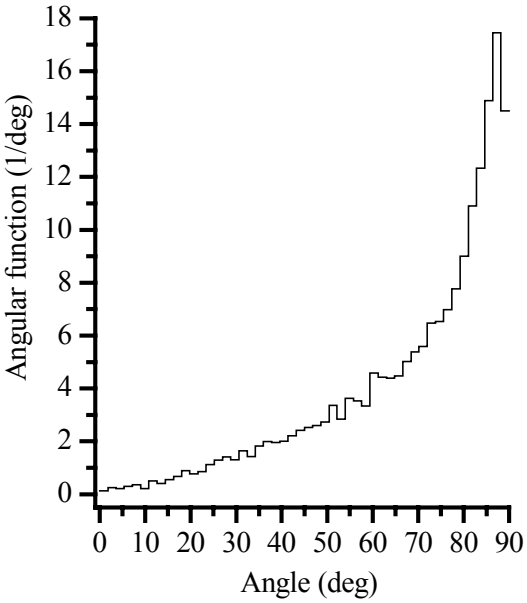

Fig. 35. Angular spectrum of electrons at the depth of 0.37 cm (after 5-th cell) in a microcircuit.

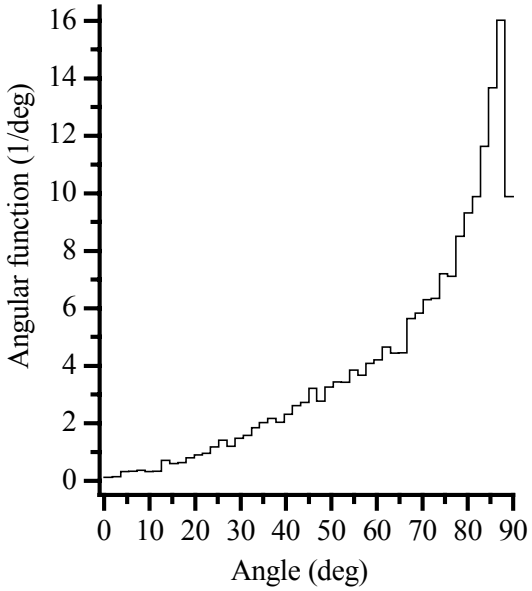

Fig. 36. Angular spectrum of electrons at the depth of 0.39 cm (after 8-th cell) in a microcircuit.

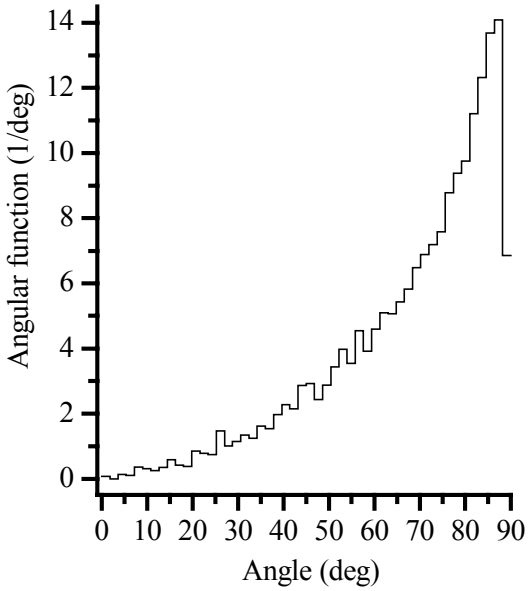

Fig. 37. Angular spectrum of electrons at the depth of 0.95 cm (after 11-th cell) in a microcircuit.

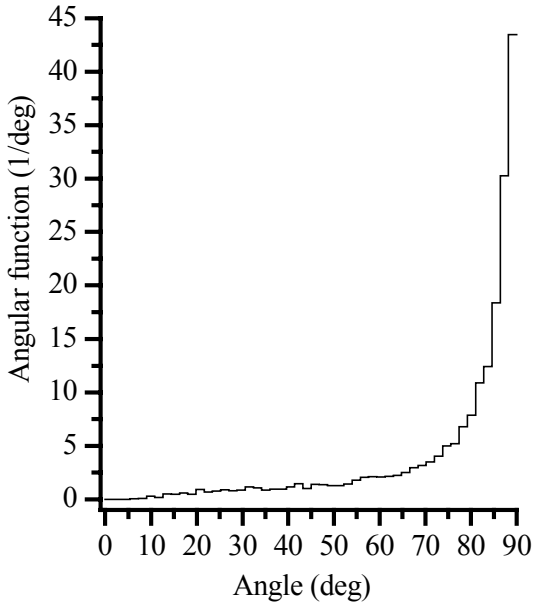

Fig. 38. Angular spectrum of photons at the depth of 0.27 cm (after 4-th cell) in a microcircuit.

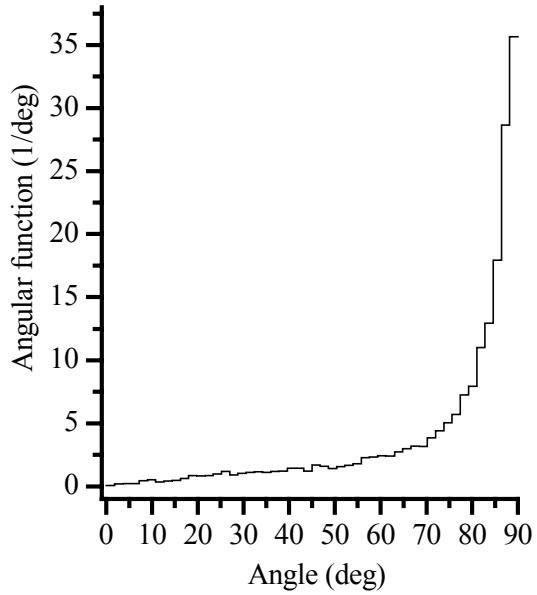

Fig. 39. Angular spectrum of photons at the depth of 0.375 cm (after 6-th cell) in a microcircuit.

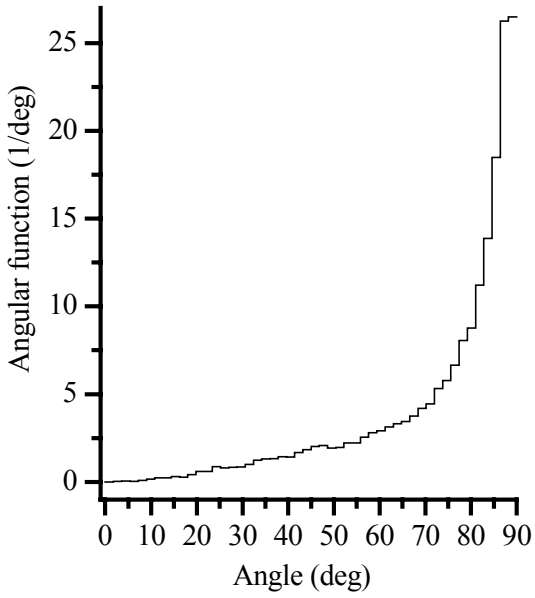

Fig. 40. Angular spectrum of photons at the depth of 0.89 cm (after 9-th cell) in a microcircuit.

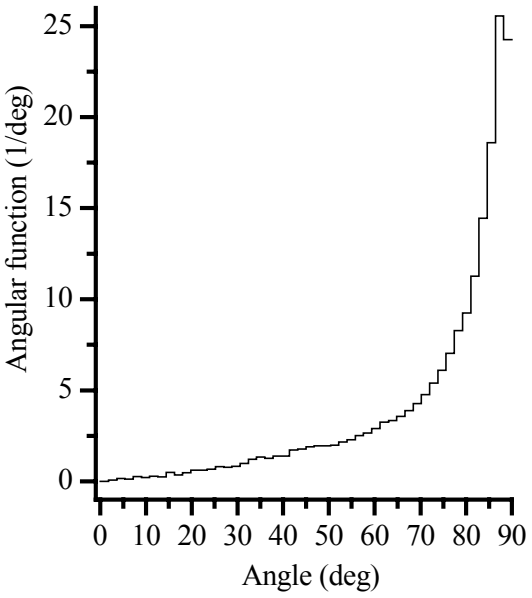

Fig. 41. Angular spectrum of photons at the depth of 0.95 cm (after 11-th cell) in a microcircuit.

Thus, presented Monte Carlo model allows to carry out the numerical experiment on passage of the photon-electron cascade through composite targets.

This work was supported by
International Science and Technology Center
under Project B-23-96

References

1. Berestetskii V.B., Lifshitz E.M., Pitaevskii L.P. Quantum Electrodynamics (in Russian), Moscow, 1980.
2. Spencer L., Coyne J.// Phys. Rev. 1962. Vol.128. P.2230-2239.
3. Gluckstern R.L., Hull M.H. Phys. Rev.1953. Vol.90. N 6. P.1030.
4. Bazylev B.N., Miloshevsky G.V., Romanov G.S., Suvorov A.E. Monte Carlo method for simulation of bremsstrahlung emission. Collected book of scientific Proceeding of IHMT (in Russian), Minsk, 1994, P.97-103.
5. Sobol' I.M. Numerical Monte Carlo Methods (in Russian), Moscow, 1973.
6. Landau L.D., Lifshitz E.M. The Classical Theory of Fields (in Russian), Moscow, 1973.
7. Bazylev B.N., Golub L.V., Romanov G.S., Tolkach V.I. Engineer-physical Journal. V.58, N.6, P.1012-1990.
8. Bazylev B.N., Golub L.V., Romanov G.S., Tolkach V.I. Engineer-physical Journal. V.59, N.1, P. 62-1990.
9. Akkerman A.F. Simulation of Paths of Charged Particles in Material (in Russian), Moscow, 1991.
10. McDonald I.R., Lamki A.M., Delaney C.F. // J. Phys. D. Appl. Phys. 1971, V.4, N.8, P.1210-1217.
11. Goudsmit S., Saunderson J.L. Multiple Scattering of Electrons. I. Phys. Rev., 1940, V.57, P.24.
12. Goudsmit S., Saunderson J.L. Multiple Scattering of Electrons. II. Phys. Rev., 1940, V.58, P.36.
13. Rossi B. High Energy Particles, New York, 1952.
14. Engelko V., Komarov O., Kovalev V., Lublin B., Wurz H., Miloshevsky G. Formation and investigation of an intense rotating electron beam and its interaction with solid materials. Proceeding of 1995 IEEE International Conference on Plasma Science. Madison, Wisconsin, USA. 5-8 june 1995, P.289.
15. Engelko V., Komarov O., Kovalev V., Landman I., Lublin B., Miloshevsky G., Wurz H. Test of divertor materials under simulated ITER plasma disruption conditions at the ELDIS electron beam facility. Proceeding of 12rd International Conference on

Plasma Surface Interaction in Controlled Fusion devices. San-Raphael France 20- 24 May 1996.
16. Nakai Y. Japan. J. Appl. Phys., 2, 743, 1963.
17. Boiko V.I., Evstegneev V.V. Introduction to high-current beam interaction physics of charged particles with matter (in Russian). Moscow, 1988.
18. Andreev Ju.A. Dissertation. Alma-Ata, 1967.
19. Goleminov N.G., Kramer-Ageev E.A. Questions of microdosimetry (in Russian). Moscow, 1982.

Gennady V. Miloshevsky

MONTE CARLO MODEL FOR NUMERICAL SIMULATION
OF COMBINED PHOTON-ELECTRON TRANSPORT
IN COMPOSITE TARGETS

Preprint No. 1

Геннадий Викентьевич Милошевский

МОДЕЛЬ МОНТЕ-КАРЛО ДЛЯ ЧИСЛЕННОГО МОДЕЛИРОВАНИЯ
СОВМЕСТНОГО ФОТОННО-ЭЛЕКТРОННОГО ПЕРЕНОСА
В СОСТАВНЫХ МИШЕНЯХ

Препринт № 1

Подписано в печать 18.04.97 г.
Формат 60x80 1/16. Бумага типогр. № 2. Офсетная печать.
Усл. печ. л. 2,5. Усл. кр. -отт. 2,6. Уч.-изд. л. 2,8.
Тираж 50 экз. Заказ № 55.

АНК “Институт тепло- и массообмена имени А.В. Лыкова” АНБ.
220072, Минск, П.Бровки, 15.

Отпечатано в типографии АНК “Институт тепло- и массообмена имени А.В. Лыкова” АНБ. 220072, Минск, П.Бровки, 15.